Imaging of Tumor Syndromes

Prem P. Batchala, MD, Thomas J. Eluvathingal Muttikkal, MD, Sugoto Mukherjee, MD*

KEYWORDS

• Cancer syndromes • Neurofibromatosis type 1 • Neurofibromatosis type 2 • Ataxia telangiectasia • Tuberous sclerosis complex • von Hippel-Lindau syndrome • Basal cell nevus syndrome • Li-Fraumeni syndrome

KEY POINTS

- Cancer predisposition syndromes affecting the central nervous system represent a diverse subgroup of lesions, including intra-axial malignant brain tumors, extra-axial nerve sheath tumors, spinal cord tumors, vascular masses, pituitary tumors, and various hamartomas, with markedly different phenotypes both within and outside the neural axis.
- Advances in knowledge of the underlying genomics and cancer pathways has enhanced understanding of the tumor behavior, resulting in improved diagnostics, better imaging screening, and better surveillance strategies.
- Imaging serves a critical role in early diagnosis, screening, and long-term follow-up of these patients, requiring specialized whole-body protocols and surveillance techniques for optimal management.

INTRODUCTION

The tumor syndromes covered here include both inheritable and noninheritable cancer syndromes. These syndromes are more appropriately referred to as cancer predisposition syndromes, because of their complex cancer pathways, and how it is passed on from one generation to the next. Well-identified genetic mutations, which often characterize these syndromes, predispose to phenotypically distinct tumors throughout the body. The syndromes present a unique challenge to oncologists and radiologists owing to multiorgan involvement, aggressive nature of the tumors, and associated endocrine abnormalities. Recent genomic characterization of these syndromes has led to revision and reclassification of the established syndromes as well as development of targeted therapies.

Screening and diagnosis for these syndromes require a plethora of advanced laboratory tests, which include comprehensive genetic testing. Multimodality, multiorgan imaging plays a quintessential role in the screening, early diagnosis, surveillance, and management of these syndromes.

Whole-Body Imaging

In addition to targeted organ-specific protocols, dedicated whole-body imaging is becoming an indispensable tool in evaluating cancer syndromes. Occasionally, whole-body imaging refers to a combination of different modalities including ultrasonography (US), computed tomography (CT), and magnetic resonance (MR) imaging, done separately. Another emerging approach is single-modality whole-body scanning to evaluate local multiorgan tumors as well as distant metastatic disease. In this scenario, whole-body MR imaging has taken precedence over whole-body CT or PET/CT, because of lack of ionizing radiation (given that many of these patients are in the

Department of Radiology and Medical Imaging, University of Virginia Health System, 1215 Lee Street, Charlottesville, VA 22903, USA
* Corresponding author. PO Box 800170, 1215 Lee Street, Charlottesville, VA 22908-0170.
E-mail address: SM5QD@hscmail.mcc.virginia.edu

Radiol Clin N Am 59 (2021) 471–500
https://doi.org/10.1016/j.rcl.2021.01.009

pediatric age group and need repeated follow-up scans), excellent soft tissue contrast, and bone marrow evaluation.[1] Single-modality imaging also has the advantage of 1-time sedation or general anesthesia when required.

MR imaging has limitations, which include cost, decreased specificity, artifacts related to patient hardware and motion, repeated gadolinium dosage and accumulation, as well as technical issues with older scanners. However, recent advances have allowed many of the limitations to be overcome, which include rolling table platforms, multiple phased array coils, parallel imaging techniques, and wider field of view (FOV). These advances have led to improvement in resolution, decreased artifacts and scan time, with reduction in the need for repeated gadolinium administration. The principles of whole-body MR scans include using series of images at multiple stations (targeting specific body parts based on the FOV and patient size), in multiple planes (usually axial and coronal planes with sagittal plane used for spine), while using a combination of sequences tailored for specific disorders. The stations include combinations such as the chest-abdomen-pelvis station, neck-chest-abdomen-pelvis station, or brain–head and neck–spine station. Typically a combination of diffusion and fluid-sensitive sequences are used, with respiratory gating for chest and antiperistaltic drugs for abdomen. Use of gadolinium is reserved for specific syndromes and clinical situations.

CANCER PREDISPOSITION SYNDROMES

Neurofibromatosis

Neurofibromatosis is a group of hereditary syndromes with tumors involving the central and peripheral nervous systems, including neurofibromatosis type 1 (NF1), neurofibromatosis type 2 (NF2), and schwannomatosis.

Neurofibromatosis Type 1

NF1, also known as peripheral neurofibromatosis and von Recklinghausen disease, is an autosomal dominant (AD) syndrome, with high penetrance and variable expressivity, with an incidence of 1 in 3000. The mutation affects the neurofibromin tumor suppressor gene located in the long arm of chromosome 17 (17q11.2). About half are inherited and the rest result from sporadic mutations. The segmental form with a limited distribution of lesions can be seen with mosaicism.[2,3] Familial spinal neurofibromatosis is a rare form, with neurofibromas affecting nerve roots bilaterally at all spinal levels, with most patients lacking the cutaneous and ocular lesions of NF.[4] The diagnostic criteria for NF1 are summarized in **Box 1**.

Neurofibromas

Neurofibromas, which are nerve sheath tumors, are the most common tumors in NF1, and can involve both superficial and deep soft tissues, including the nerve roots in the spinal canal and neural foramen. Morphologic subtypes include localized neurofibroma, plexiform neurofibroma (PNF), and diffuse neurofibroma.[5]

Localized cutaneous neurofibroma is the most common form, presenting as nodular or polypoid lesion often with epidermal hyperpigmentation. Localized intraneural neurofibroma causes fusiform enlargement of the affected nerve.[5] The lesions appear hypodense with minimal enhancement in CT scans, well defined and hyperintense on T2-weighted imaging (T2WI), with intermediate to low signal intensity on T1-weighted imaging (T1WI), with homogeneous, slightly heterogeneous, or central enhancement (**Figs. 1** and **2**). The lesions may show target sign with low central signal with peripheral high signal in T2WI (see **Fig. 2**), and a central dense area on CT. Target sign can sometimes also be seen with schwannoma and malignant peripheral nerve tumors. Neurofibroma is challenging to differentiate from schwannoma by imaging. T2 hyperintense rim and intratumoral cysts are more common with schwannoma than with neurofibroma.[3,6]

PNF is virtually pathognomonic of NF1, and appears as lobulated, tortuous thickening of nerves with a bag-of-worms appearance (**Fig. 3**). The lesion appears as an infiltrative multispatial soft tissue density lesion in CT (**Fig. 4**). Target sign is commonly seen (see **Fig. 4**). The lesion has intermediate signal intensity in T1-weighted images, with central dotlike or diffuse heterogeneous enhancement (see **Figs. 3** and **4**).[3,5]

Box 1
National Institutes of Health Consensus criteria for neurofibromatosis type 1 diagnosis

Diagnostic criteria of NF1: 2 or more of the following criteria should be met:

1. At least 6 café-au-lait macules (diameter>5 mm in prepubertal individuals and >15 mm in postpubertal individuals)
2. Freckling in axillary or inguinal regions
3. Optic glioma
4. At least 2 Lisch nodules (iris hamartomas)
5. At least 2 neurofibromas of any type, or 1 plexiform neurofibroma
6. A distinctive osseous lesion (sphenoid dysplasia or tibial pseudarthrosis)
7. A first-degree relative with NF1

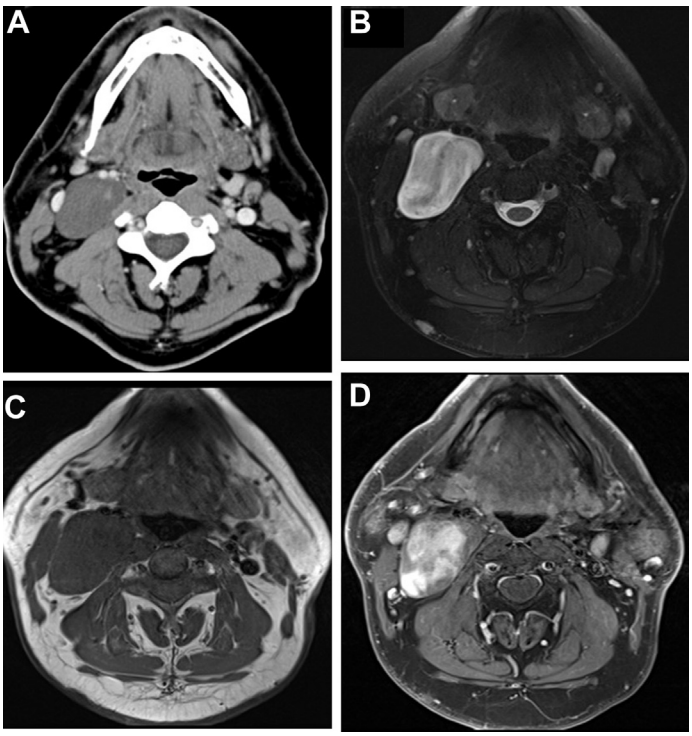

Fig. 1. Sympathetic trunk neurofibroma in a 47-year-old male patient with NF1. (*A*) Contrast-enhanced CT shows a well-defined low-density mass in the right carotid space with minimal enhancement. (*B*, *C*) On axial fat-suppressed T2WI and T1WI, the mass is hyperintense and isointense compared with muscle. (*D*) Contrast-enhanced fat-suppressed axial T1WI shows heterogeneous enhancement in the mass.

Diffuse neurofibromas most commonly occur in children and young adults as plaquelike or infiltrative, poorly defined, reticulated lesions in skin and subcutaneous fat.[3]

Malignant peripheral nerve sheath tumor

Malignant peripheral nerve sheath tumors (MPNSTs) usually arise from plexiform neurofibromas, and less commonly from localized neurofibromas. Malignant transformation of neurofibroma is often associated with rapid growth and worsening pain. Infiltrative margin, heterogeneous enhancement with necrotic areas, peripheral edema, and osseous destruction are features suggestive of malignant transformation (**Fig. 5**). MPNST shows high ^{18}F-fluorodeoxyglucose

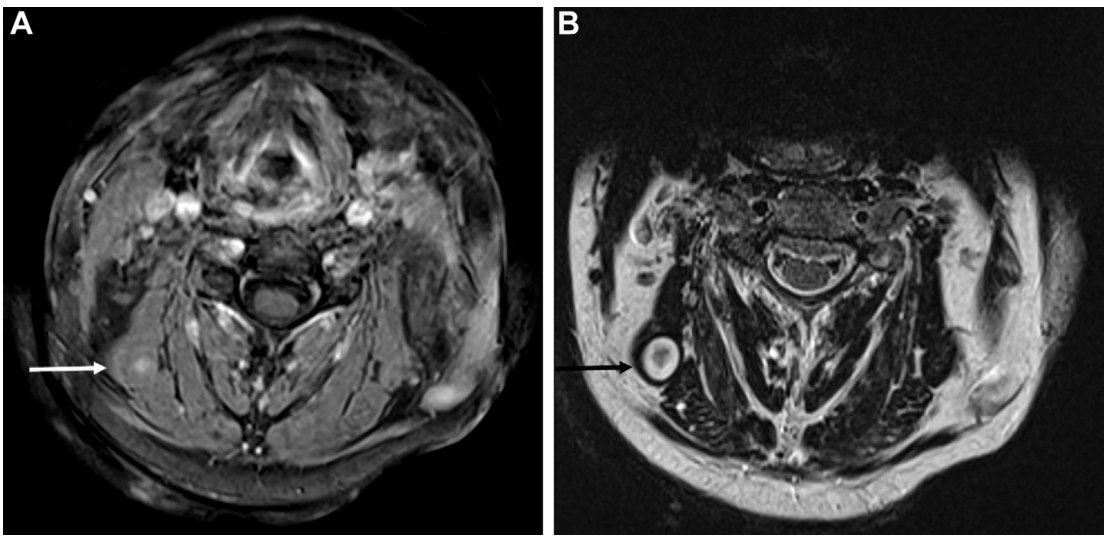

Fig. 2. Neurofibroma in a 54-year-old man with NF1. (*A*) Contrast-enhanced axial fat-suppressed T1WI shows central enhancement in an intramuscular neurofibroma (*white arrow*). (*B*) Axial T2WI shows target sign with central T2 hypointensity (*black arrow*).

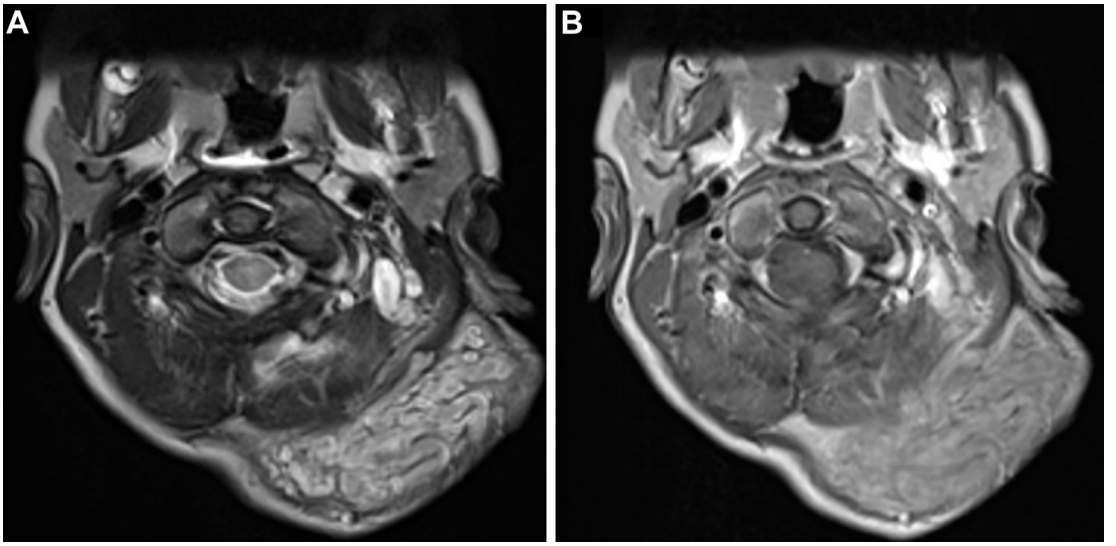

Fig. 3. Plexiform neurofibroma in a 12-year-old female patient with NF1. (*A*) Axial T2WI shows bag-of-worms appearance in the left suboccipital region. (*B*) Contrast-enhanced axial T1-weighted image shows diffuse heterogeneous enhancement.

(FDG) uptake on PET scans. About half of the MPNSTs occur in patients with NF1, and about 5% of patients with NF1 develop MPNST.[2,3]

Optic pathway gliomas

NF1-associated optic pathway glioma (OPG) typically presents in young children. OPGs usually are low-grade pilocytic astrocytomas.[2] Less than half of the cases are symptomatic. OPG in patients with NF1 commonly involves the optic nerve, followed by the chiasm, unlike OPG in patients without NF1. Hypothalamic involvement can present with premature or delayed puberty.[7]

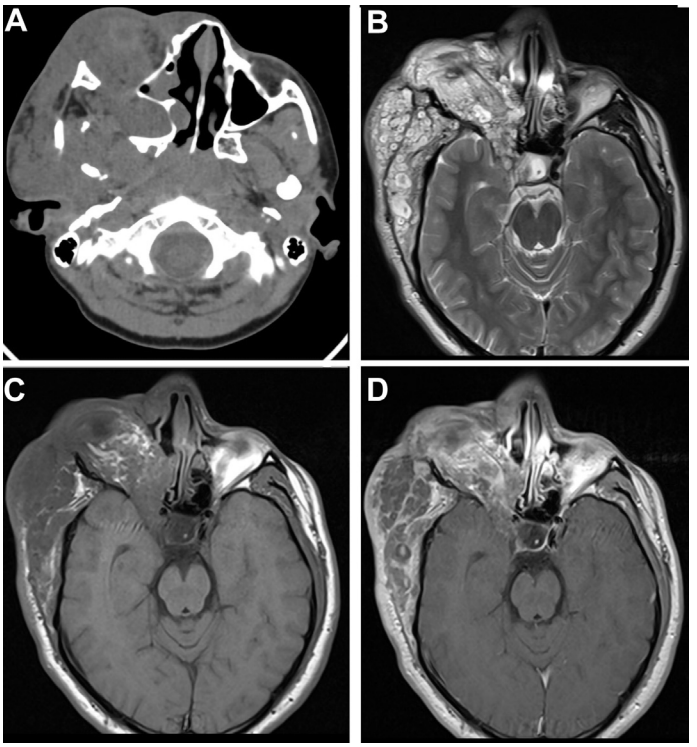

Fig. 4. Plexiform neurofibroma in a 17-year-old male patient with NF1. (*A*) Axial CT scan shows an infiltrative multispatial soft tissue density mass in right side of the face and temporal fossa. (*B*) Axial T2WI shows multiple target sign within the plexiform neurofibroma. (*C*) Axial T1WI and (*D*) postcontrast T1WI show intermediate signal lesion with heterogeneous enhancement.

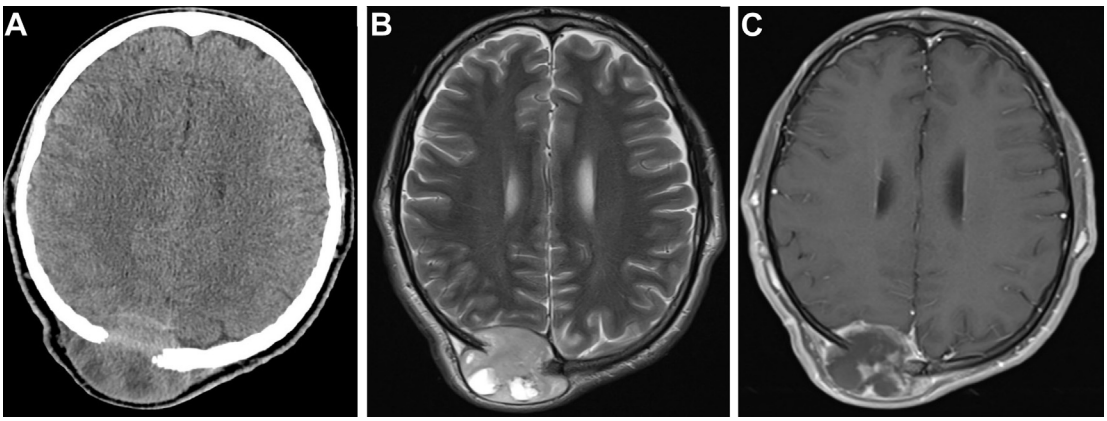

Fig. 5. Rapidly growing right parietal scalp mass in a 28-year-old man with NF1. (*A*) Axial contrast-enhanced CT, (*B*) axial T2WI, and (*C*) postcontrast T1WI show heterogeneously enhancing mass with cysts and necrosis. There is also calvarial destruction by the mass.

OPG appears as fusiform enlargement of the nerve that is isodense to slightly hypodense on CT scans. The optic canal may appear enlarged. Calcification is rare, which helps to differentiate OPG from optic sheath meningioma. OPG appears hyperintense on T2WI, and shows variable contrast enhancement (Fig. 6). Cysts are uncommon in OPG associated with NF1.[7,8]

Other central nervous system and extra–central nervous system tumors

Brainstem gliomas are the second most common intracranial tumors in NF1 (Fig. 7), frequently pilocytic astrocytomas with few transforming into aggressive gliomas (Figs. 8 and 9). There is increased risk of rhabdomyosarcomas, gastrointestinal stromal tumors, endocrine tumors of gastrointestinal tract, pheochromocytomas, breast cancer, and hematopoietic malignancies.[2]

Other neuroimaging findings

An unusual but characteristic imaging finding, known as focal abnormal signal intensity (FASI), can be seen in basal ganglia, thalamus, pons, midbrain, cerebellar peduncles, cerebellar white matter, dentate nuclei, and less commonly supratentorial white matter, likely from myelin vacuolization (Fig. 10). These findings are usually hyperintense on T2WI, isointense on T1WI, with a few appearing mildly hyperintense on T1 in basal

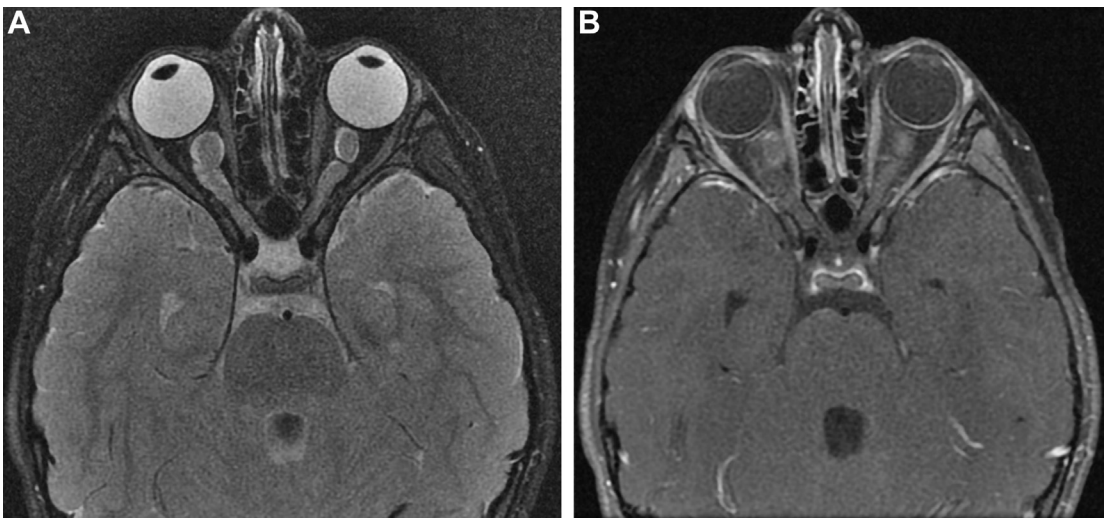

Fig. 6. Bilateral optic glioma in a 5-year-old female patient with NF1. (*A*) Axial fat-suppressed T2WI shows fusiform enlargement of bilateral optic nerves. (*B*) Contrast-enhanced axial fat-suppressed T1WI showing mild enhancement of enlarged optic nerves.

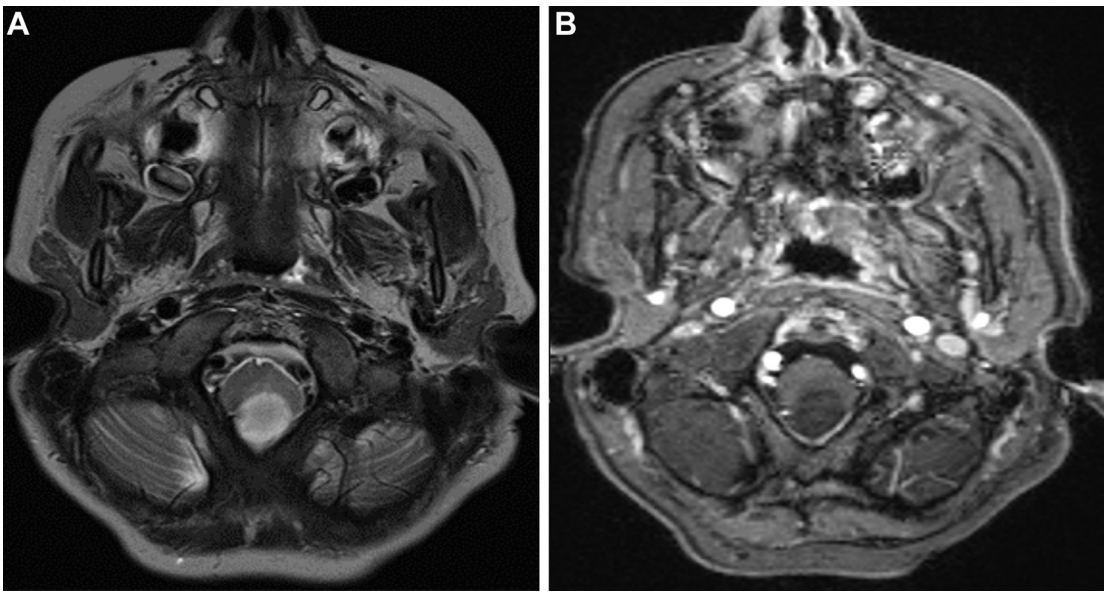

Fig. 7. Exophytic brainstem glioma in an 8-year-old boy with NF1. (*A*) Axial T2WI shows a well-defined hyperintense exophytic dorsal brainstem. (*B*) Contrast-enhanced magnetization prepared rapid gradient echo (MPRAGE) T1WI shows no enhancement in the mass.

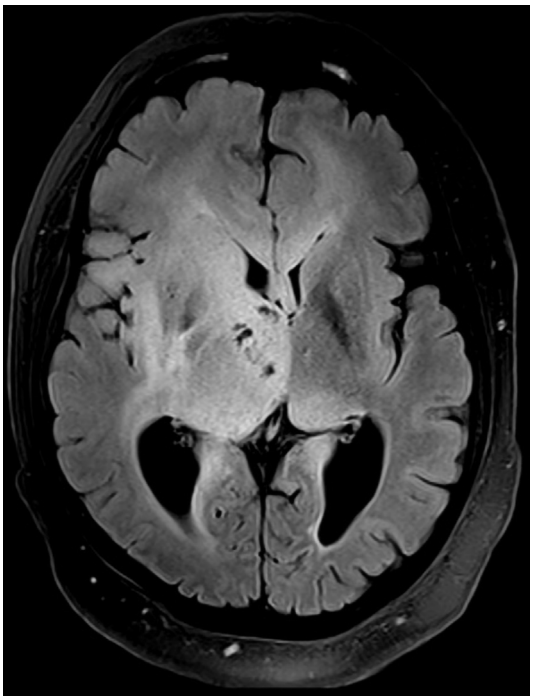

Fig. 8. Diffuse infiltrative astrocytoma in a 21-year-old man with NF1. Axial fluid-attenuated inversion recovery (FLAIR) image shows a diffuse infiltrative tumor involving the right basal ganglia, right thalamus, left thalamic pulvinar, right insular cortex, corpus callosum, and periventricular white matter.

ganglia, likely because of microcalcifications. Although they typically have no associated mass effect or enhancement, rarely they show mild mass effect in basal ganglia. FASI can become bigger in early childhood before they regress.[9,10] Cerebrovascular dysplasia including stenosis, hypoplasia, moyamoya pattern (**Fig. 11**), and aneurysms can occur.[11]

Neurofibromatosis Type 2

Just like NF1, NF2 is also an AD genetic syndrome, with high penetrance and variable expressivity. However, it is rarer, with an incidence of 1 in 25,000. NF2 results from a mutation of the NF2 gene, which codes for the cytoskeletal protein schwannomin (merlin) located on chromosome 22 (22q12.2), which acts as a tumor suppressor protein. About half of the cases have de novo mutation, with somatic mosaicism in about one-third of these cases.[2]

The diagnostic criteria for NF2 are summarized in **Box 2**. The 1987 National Institute of Health (NIH) criteria were modified to include patients with multiple schwannomas and or meningiomas with no family history and who have not yet developed bilateral eighth nerve tumors. These criteria include the Manchester criteria, National Neurofibromatosis Foundation (NNFF) criteria, and Baser criteria[12] (**Box 3**). Young patients (<18 years old) with apparently isolated meningioma or vestibular schwannoma have a 20% and 10% likelihood,

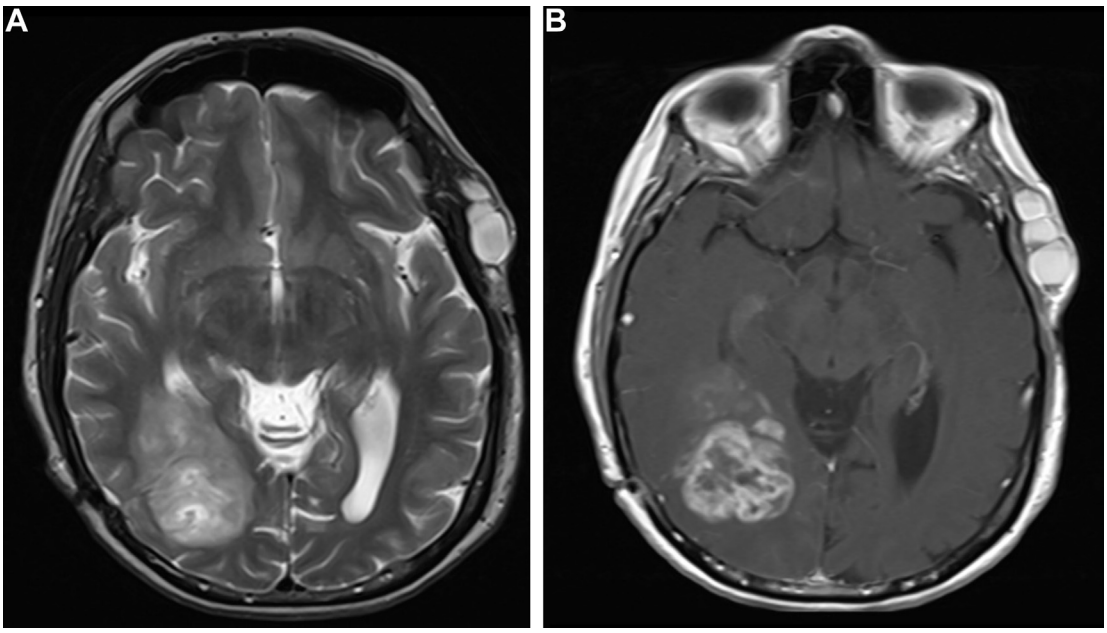

Fig. 9. High-grade glial tumor in a 42-year-old woman with NF1. (*A*) Axial T2WI and (*B*) postcontrast T1WI show a heterogeneously enhancing right posterior temporo-occipital lobe tumor.

respectively, of developing NF2. After 20 years, likelihood decreases, and NF2 becomes very unlikely after 30 years.[13] In contrast, 50% of patients more than 70 years of age with bilateral vestibular schwannoma without other features of NF2 represent a chance occurrence rather than underlying mosaic or constitutional NF2 mutation.[14]

Schwannomas

In addition to bilateral vestibular schwannomas (**Fig. 12**A, B) usually occurring by 30 years of age in about 90% to 95% of patients, schwannomas of other cranial nerves are present in up to about half of the patients (**Fig. 12**C). Unilateral hearing loss and tinnitus are the presenting symptoms in

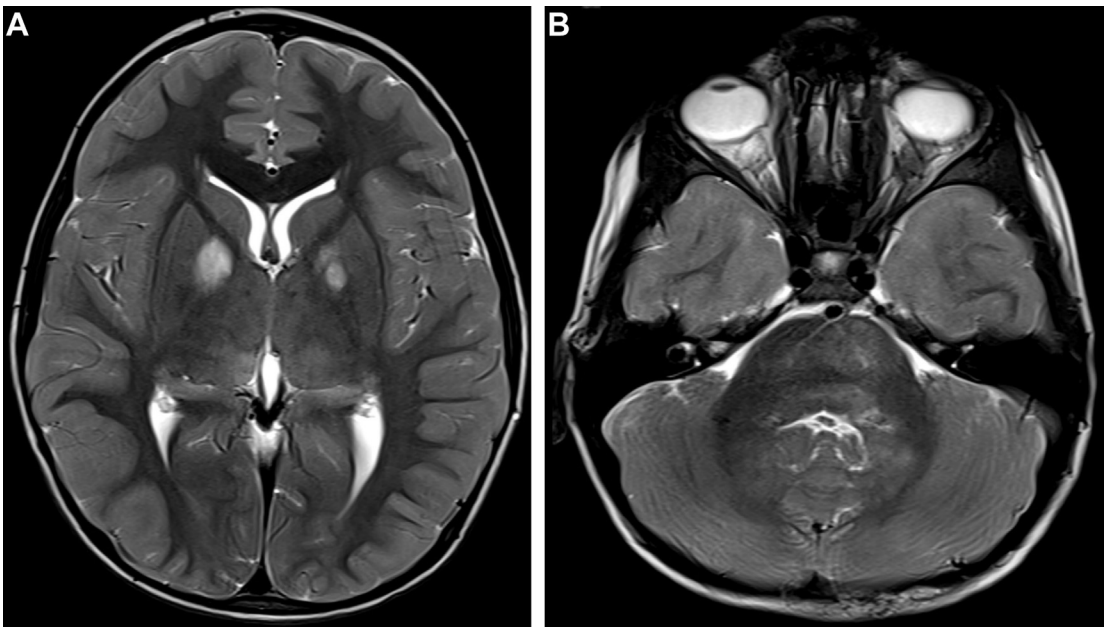

Fig. 10. FASI in a 7-year-old boy with NF1. Axial T2WI at the level of (*A*) basal ganglia and (*B*) pons show hyperintense foci in bilateral globus pallidi, dorsomedial thalami, pons, cerebellar peduncles, cerebellar white matter, and dentate nuclei.

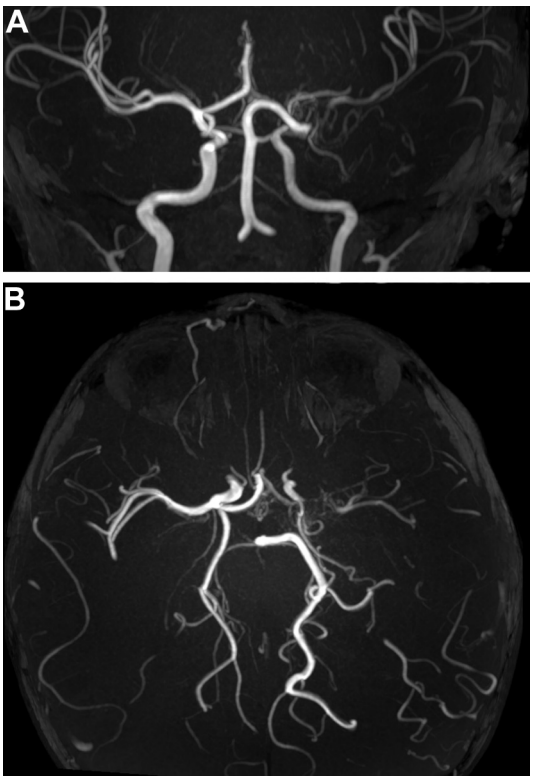

Fig. 11. Moyamoya pattern in a 9-year-old girl with NF1. (*A*) Coronal and (*B*) axial maximum intensity projections of three-dimensional (3D) time-of-flight MR angiography (MRA) head show occlusion of left intracranial internal carotid artery with prominent left sided lenticulostriate collaterals (moyamoya or puff-of-smoke pattern).

more than half of the adults and about a quarter of the children.[15] Schwannomas can also affect spinal (**Fig. 13**) and peripheral nerves. Vestibular schwannomas appear as enhancing masses that are ovoid when small, and ice cream cone–shaped when large enough to extend in to the cerebellopontine angle from the internal auditory canal (IAC). These lesions show up as filling defects within the cerebrospinal fluid (CSF) on high-resolution heavily T2-weighted sequences (see **Fig. 12**). CT scan shows widening of the IAC, whereas the tumor may be difficult to see on soft tissue windows.

Box 2
National Institutes of Health criteria for neurofibromatosis type 2 diagnosis

A patient who meets either condition A or B has NF2.

A. Bilateral vestibular schwannomas

B. First-degree family relative with NF2 and unilateral vestibular schwannoma or any 2 of neurofibroma, meningioma, glioma, schwannoma, or juvenile posterior subcapsular lenticular opacity

Box 3
Revised Manchester criteria for neurofibromatosis type 2

A patient who meets any 1 of the following criteria has NF2:

1. Bilateral vestibular schwannomas if less than 70 years of age.
2. First-degree relative with family history of NF2 (excluding siblings with clearly unaffected parents) and unilateral vestibular schwannoma if less than 70 years of age.
3. First-degree relative with family history of NF2 or unilateral vestibular schwannoma and 2 of the following lesions: meningioma, ependymoma, schwannoma, cataract, cerebral calcification. LZTR1 (leucine-zipperlike transcription regulator 1) test has to be negative, if unilateral vestibular schwannoma plus $\geq$2 nonintradermal schwannomas.
4. Multiple meningiomas (2 or more) and 2 of unilateral vestibular schwannoma, schwannoma, cataract, cerebral calcification.
5. Constitutional pathogenic NF2 gene variant in blood or identical in 2 tumors.

Meningiomas

Intracranial meningiomas are present in about half of the patients, and spinal meningiomas are present in about 20%. Although many of these lesions remain asymptomatic, larger lesions, as well as smaller lesions within the spinal canal, optic canal, or skull base, can be symptomatic.[15] They appear as extra-axial masses, usually with intense contrast enhancement (see **Fig. 12**; **Fig. 14**), similar to sporadic meningiomas.

Ependymomas

Ependymomas are present in up to about half of patients, mostly within the upper cervical canal or at the craniocervical junction. On imaging, these look similar to their sporadic counterparts, including showing hemosiderin cap and homogeneous enhancement (see **Fig. 14**).[15]

Other central nervous system tumors

Intramedullary astrocytomas and schwannomas of the spinal cord and meningioangiomatosis have also been reported in NF2.[15,16]

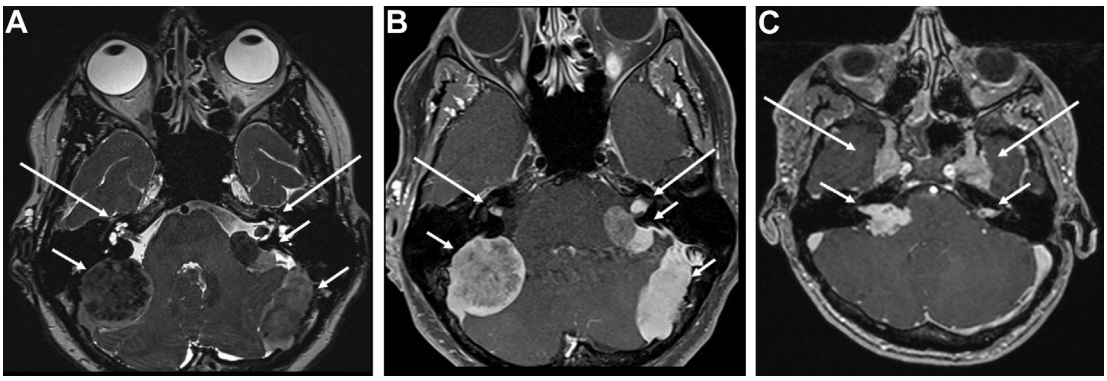

Fig. 12. NF2. (*A*) Axial high resolution heavily weighted T2 and (*B*) contrast-enhanced fat-suppressed axial T1WI at the level of internal auditory canals in a 60-year-old man with NF2 show T2-hypointense enhancing bilateral vestibular schwannomas (*long arrows*) and multiple posterior fossa meningiomas (*short arrows*). The low T2 signal in the meningiomas reflects calcification. (*C*) Contrast-enhanced axial MPRAGE image in a 42-year-old woman with NF2 shows bilateral vestibular (*short arrows*) and trigeminal schwannomas (*long arrows*).

Schwannomatosis

Schwannomatosis is the third major form of neurofibromatosis, with an incidence of 1 in 60,000 to 70,000, characterized by multiple schwannomas without evidence of bilateral vestibular schwannomas. Inheritance is AD, with a sporadic predominance. The tumor suppressor genes identified are SMARCB1 (SWI/SNF-Related Matrix-associated Actin-dependent Regulator of Chromatin Subfamily B Member 1) and *LZTR1* (leucine-zipperlike transcription regulator 1), located in the long arm of chromosome 22.[17] The diagnostic criteria for schwannomatosis are summarized in **Box 4**.[17] The overlap in presentation and phenotype of schwannomatosis and NF2 makes the clinical differentiation difficult. On imaging, the schwannomas look identical to those in NF2. Spinal ependymomas are not present in schwannomatosis, which helps in differentiating from NF2.

von Hippel-Lindau Syndrome

von Hippel-Lindau (VHL) is an AD syndrome arising from mutations in the VHL tumor suppressor gene located in chromosome 3 (3p25-26). The mutation causes overexpression of hypoxia-inducible messenger RNAs, including vascular endothelial growth factor, which results in angiogenesis, and proliferation of endothelial cells and pericytes that are characteristic of VHL-related tumors. Hemangioblastoma (HB) and endolymphatic sac tumor (ELST) are the most common central nervous system (CNS) tumors in VHL, with rare reports of choroid plexus papilloma. The average age of presentation of VHL-related tumors is the third to fourth decade.[18] Tumor combinations in VHL often overlap with other syndromes, such as NF1 and multiple endocrine neoplasia (MEN) and pose a diagnostic challenge.[18] The recommended diagnostic criteria by the Danish VHL coordination group are summarized in **Box 5**.[18] The recommended NIH screening guidelines for VHL tumors are summarized in **Table 1**.[19]

Central nervous system hemangioblastoma

CNS hemangioblastomas (HBs) are World Health Organization (WHO) grade I tumors that present at a younger age in VHL compared with their sporadic counterparts. Their frequency varies along the craniospinal axis, with cerebellar being most common (44%–72%), followed by brainstem (10%–25%), spinal cord (13%–50%), cauda equina (<1%), and supratentorial compartment (<1%).[20] HBs vary in size at the time of presentation. Early symptomatic HBs tend to have larger cystic components and often present with headache, cerebellar signs, cranial nerve palsies, or cord compression. Wanebo and colleagues[21] in their series of 160 patients reported more frequent association of cysts in symptomatic cerebellar HB than in asymptomatic cases (72% vs 13%, $P<.0001$). In close to 80% of VHL cases, HBs are multifocal.[21]

HBs are best evaluated by MR imaging and present as cyst with a mural nodule (most common type) or a solid nodule without or with internal cystic change (**Fig. 15**A).[22,23] Pure cystic morphology is very rare. The nodule shows intense postcontrast enhancement with characteristic superficial or pial location, and predilection to the posterior aspects of cerebellum, brainstem, and spinal cord. The nodule is isointense to

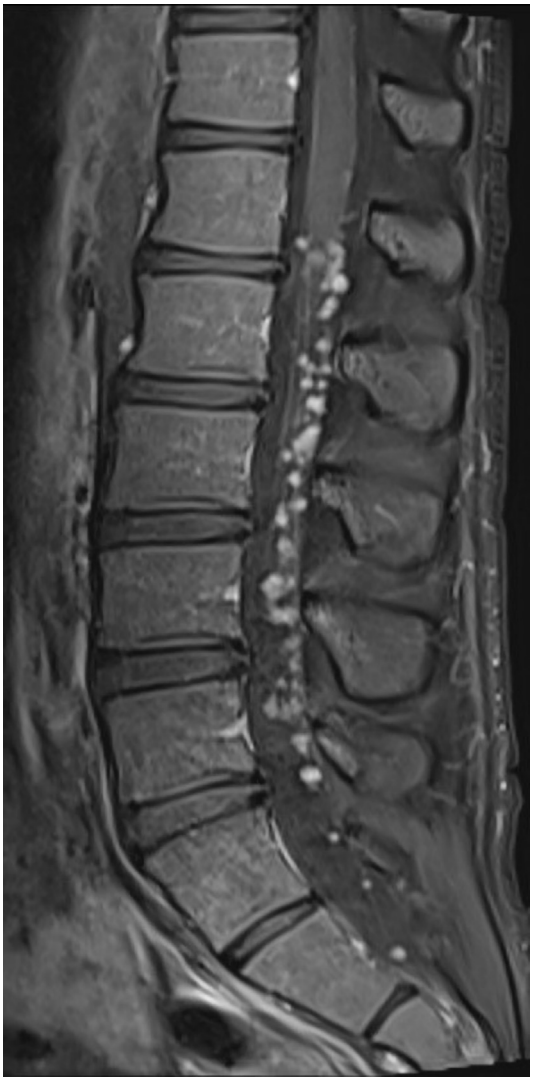

Fig. 13. Numerous enhancing cauda equina nerve root schwannomas seen in this sagittal fat-suppressed postcontrast T1WI of the lumbar spine in a 21-year-old man with NF2.

hypointense on T1WI and hyperintense on T2WI. The cystic component is usually hyperintense to CSF on T1WI and fluid-attenuated inversion recovery (FLAIR). Vasogenic edema may be seen around the HB (Fig. 15B). Flow voids or prominent vessels around the HB indicates its vascular nature (Fig. 16). Catheter angiography is not required for the diagnosis and can also display intense prolonged contrast staining of the nodules with arteriovenous shunting (Fig. 15C). Spinal cord HBs also show similar imaging features. In addition, a syrinx may be seen.[23] In patients with VHL, renal cell carcinoma (RCC) CNS metastasis should always be considered in the differential diagnosis. RCC metastasis can mimic HB on histopathology and also on imaging.

Retinal hemangioblastomas

Retinal HBs are seen in 52% to 84% of VHL cases and can be the only presentation in as many as 11%.[18,20,24,25] In 50%, they are multifocal and bilateral. Most are asymptomatic with a limited role for imaging. If seen on MR imaging, HBs are mildly hyperintense on T1WI relative to vitreous with intense postcontrast enhancement (Fig. 17).

Endolymphatic sac tumor

ELST is seen in 11% of VHL cases, and the average age of presentation is 22 years.[20] It is a locally aggressive, slow-growing neoplasm arising from endolymphatic sac housed in the posterior aspect of the petrous bone and has low metastatic potential. Akin to vestibular schwannoma in NF2, bilateral ELST is pathognomonic of VHL. Bilateral tumors are seen in 30% of patients with VHL.[26] The presenting symptoms vary between hearing loss, tinnitus, imbalance, and facial nerve palsy.

Contrast-enhanced MR imaging and/or CT are typically used for diagnosing ELST. Small lesions may not be readily apparent on CT (Fig. 18). Larger lesions typically show a moth-eaten type of osteolysis with spiculated tumor matrix calcification.[23] Intense enhancement can be seen in the soft tissue component. On MR imaging, the soft tissue shows heterogeneous signal, mildly hyperintense on T1WI (because of hemorrhage) and hyperintense on T2WI and FLAIR sequences. Stippled or paint-brush pattern of enhancement has also been described on MR imaging[27] (Fig. 19). In the setting of VHL, it is important to remember that paraganglioma or metastatic carcinoma can also appear similar on imaging.

Tuberous Sclerosis

Tuberous sclerosis (TS) is an AD syndrome linked to mutations in TS complex (TSC) 1 and TSC2 genes in chromosomes 9q34 and 16p13.3 respectively.[28] TSC1 and TSC2 genes code for hamartin and tuberin proteins respectively, which together form a heterodimer that inhibits mammalian target of rapamycin (mTOR) pathway. Mutations activate the mTOR pathway, which causes unregulated cellular growth and formation of CNS and extra-CNS hamartomas. The classic TS clinical triad is epilepsy, mental retardation, and facial angiofibromas. Other CNS-related symptoms include cognitive dysfunction, neuropsychiatric abnormalities, or increased intracranial pressure caused by obstructive hydrocephalus from subependymal giant cell astrocytoma (SGCA). The diagnostic criteria recommended by the 2012 International

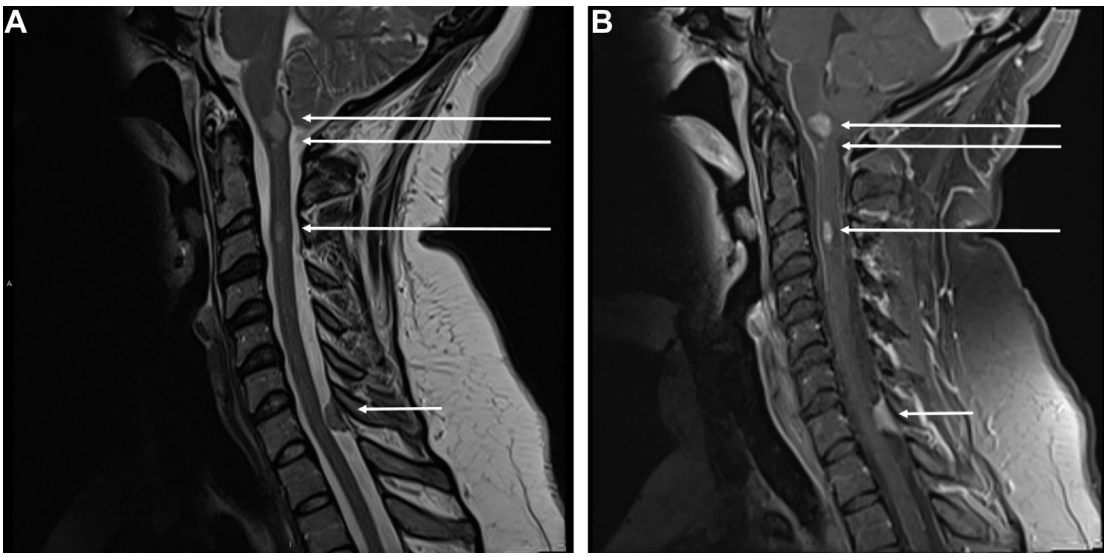

Fig. 14. Spinal ependymoma and meningioma in a 32-year-old patient with NF2. (*A*) Sagittal T2WI and (*B*) fat-suppressed postcontrast T1WI show intramedullary T2-hyperintense enhancing ependymomas (*long arrows*) and extramedullary intradural T2 intermediate signal enhancing meningiomas (*short arrow*).

Tuberous Sclerosis Complex Consensus Group are summarized in **Table 2**.[29] CNS manifestations of TS include cortical/subcortical tubers, radial migration lines, subependymal nodules (SENs), and SGCA, and each constitutes a major feature in the diagnostic criteria.

Cortical/subcortical tubers, radial migration lines

Tubers are hamartomas that arise from abnormal neuronal migration, differentiation, and organization and are seen in 95% of patients with TS.[30] Tubers are cortical/subcortical in location with supratentorial and frontal lobe predominance. Cerebellar tubers have been reported in 12% to 30% of cases.[30,31] Number and size of the tubers vary in individual patients. Tubers typically expand the affected gyri with mushroomlike or wartlike protrusions.

Imaging appearance and conspicuity of tubers are partly influenced by the degree of myelination.

Box 4
Diagnostic criteria for schwannomatosis

A patient should meet the following criteria for a diagnosis of schwannomatosis:

1. Anatomically distinct 2 nonintradermal schwannomas, 1 of which has to be histologically confirmed.
2. No evidence of bilateral vestibular schwannomas on imaging or NF2 mutation.
3. Presence of 1 pathologically confirmed schwannoma, unilateral vestibular schwannoma, or intracranial meningioma and schwannomatosis in a first-degree relative.

Box 5
Danish diagnostic criteria for von Hippel-Lindau

VHL diagnostic criteria: positive if individual satisfies criteria 1 or 2 or both	
Criterion 1	At least 2 manifestations stated below
Criterion 2	At least 1 manifestation stated below plus pathogenic mutation of VHL (or) at least 1 first-degree relative with VHL
VHL manifestations that satisfy criteria	
Retina	Hemangioblastoma
CNS	Hemangioblastoma of cerebellum, medulla oblongata, and/or spinal cord
Temporal bone	Endolymphatic sac tumor
Kidney	Renal cell carcinoma
Pancreas	Neuroendocrine tumor and/or multiple cysts
Adrenal gland/ sympathetic chain	Pheochromocytoma, paraganglioma, and/ or glomus tumor

Table 1
Screening recommendations for central nervous system tumors of von Hippel-Lindau

Tumor	Screening Recommendation
CNS hemangioblastoma	MR imaging of brain and spine every 2 y starting from 11 y of age
Retinal hemangioblastoma	Annual ophthalmoscopy starting from infancy
Endolymphatic sac tumor	Annual audiometry starting from 5 y of age and, if abnormal, dedicated temporal bone MR imaging/CT

In general, the thickened peripheral cortex is isointense to gray matter on T1WI and T2WI. The inner core of the tuber is hypointense on T1WI and hyperintense on T2WI/FLAIR, and sometimes appears cystic[32](**Fig. 20**A, B). In infants less than 6 months old, because of the lack of myelination, the tuber can appear hyperintense on T1WI and hypointense on T2WI. Postcontrast enhancement is a rare feature seen in less than 5% of tubers.[30] Tubers show facilitated diffusion, and the ones with higher apparent diffusion coefficient (ADC) values can be epileptogenic. On CT, the subcortical components of the tubers are seen as hypodense areas, which can become isodense over time. Altman and colleagues[33] reported tuber calcifications in 54% of cases on CT.

Cerebellar tubers differ from supratentorial lesions in their imaging appearance.[31] The lesions appear dystrophic rather than dysplastic, and show wedge-shaped morphology like infarcts. Folial retraction can be present, and calcifications and enhancement are more frequent (**Fig. 21**). Cerebellar lesions have been linked to TSC2 mutations. Cerebellar lesions are most frequent in the posterior lobe.

Radial migration lines are wedge-shaped, straight, or curvilinear lines extending from periventricular white matter toward the cortex, often toward the tuber like a comet tail (**Fig. 20**C). These lines represent heterotopic glial and neuronal cells along the migratory pathway. On MR imaging, the lines are isointense to hypointense on T1WI and hyperintense on T2WI/FLAIR.

Subependymal nodules and subependymal giant cell astrocytoma

SENs are also hamartomas, located along the ependyma, and are seen in 95% of patients with TS.[30] There is a strong predilection to caudate nucleus and caudothalamic groove, but they can be found at other locations, including the third and fourth ventricles. SENs measure 1 to 12 mm and show no growth in longitudinal studies. On MR, SENs appear mildly hyperintense on T1WI and isointense to hyperintense on T2WI/FLAIR sequences. Calcification is seen in 88% as low signal on susceptibility-weighted imaging (SWI). Enhancement is present in 30% to 80% and is not a sign for transformation into SGCA (**Fig. 22**).

SENs larger than 13 mm or that continue to grow are considered as imaging criteria for

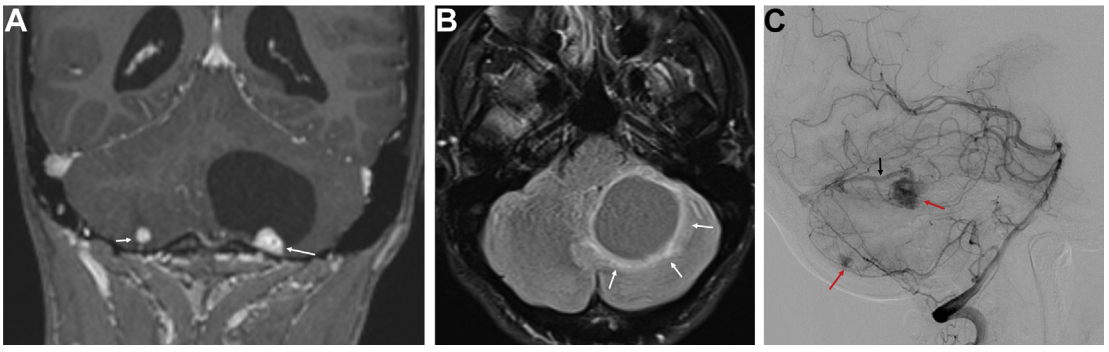

Fig. 15. Hemangioblastomas in a 20-year-old male patient with VHL. (*A*) Postcontrast T1WI showing cerebellar HBs. Cyst with a mural nodule morphology in left cerebellum (*long arrow*) and solid morphology in right cerebellum (*short arrow*). Nodules show intense postcontrast enhancement with superficial/pial location. (*B*) Vasogenic edema around the nontumor cystic component of the left cerebellar HB (*arrows*). (*C*) Catheter angiography after vertebral artery injection shows cerebellar HBs (*red arrows*) as focal intense staining with venous shunting (*black arrow*).

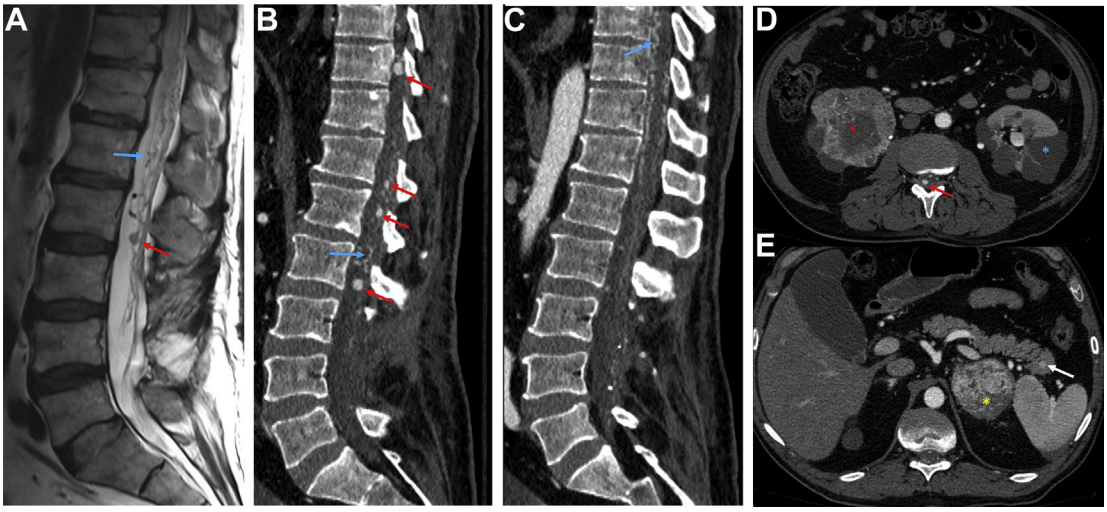

Fig. 16. A 55-year-old man with a known diagnosis of VHL. (*A*) Sagittal T2WI. (*B*, *C*) Sagittal reformations of postcontrast abdominal CT show multiple HBs (*red arrows*) along the conus and cauda equine roots. Flow voids on T2WI (*blue arrows*) and corresponding enhancing tortuous vessels on CT are also present. (*D*, *E*) Axial postcontrast abdomen CT show multiple renal cysts (*blue asterisk*), right renal cell carcinoma (*red asterisk*), left pheochromocytoma (*yellow asterisk*), and pancreatic tail neuroendocrine tumor (*white arrow*).

SGCA. SGCA is the most common CNS tumor (WHO grade I) in patients with TS, seen in 10% to 15%.[34] SGCAs are most commonly detected during early childhood (5–10 years), and are presumed to arise from a preexisting SEN.[35] They are typically found along the lateral ventricular wall, near the foramen of Monro, can be unilateral or bilateral, and can cause obstructive hydrocephalus. SGCAs show heterogeneous signal on MR. They are predominantly hypointense to white matter on T1WI and hyperintense on T2WI (**Fig. 23**).[35] Flow voids can be seen in the tumor with bright postcontrast enhancement indicating vascularity. Rarely, intraventricular hemorrhage arises from SGCA.[36] Sener[37] reported ADC values in SGCA to be similar to normal white matter (0.89×10^{-3} mm^2/s). Like other brain neoplasms, SGCA can show high choline/creatine ratio and low N-acetyl aspartate (NAA)/creatine ratio on MR spectroscopy (**Fig. 24**).[38] Symptomatic SGCAs are managed by surgical resection. mTOR pathway inhibitors (eg, everolimus) are used in nonsurgical candidates.

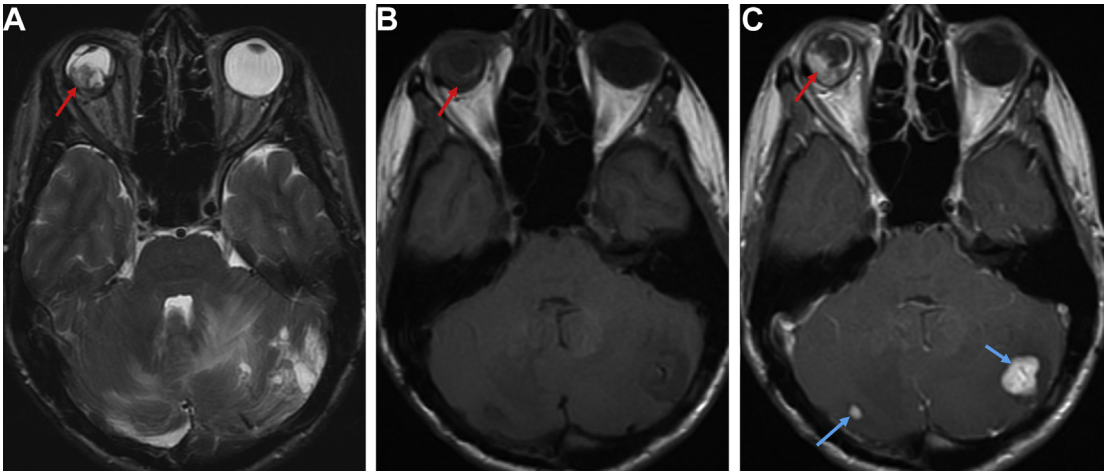

Fig. 17. A 39-year-old man with VHL and blind right eye. (*A*) Axial T2WI, (*B*) T1WI, and (*C*) postcontrast T1WI show retinal HB in right globe (*red arrow*). The mass shows T1 shortening and intense postcontrast enhancement. Cerebellar HBs are also seen (*blue arrows*), consistent with VHL.

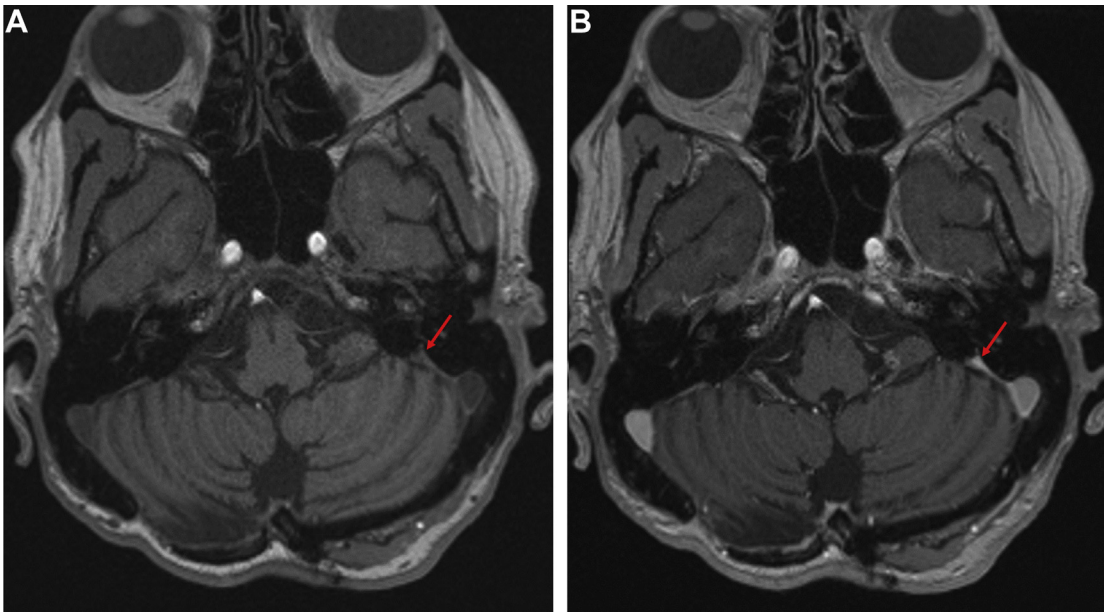

Fig. 18. A 69-year-old woman with VHL. (*A*) Axial T1WI and (*B*) postcontrast T1WI show focal enhancement in left endolymphatic sac compatible with early endolymphatic sac tumor (*red arrows*).

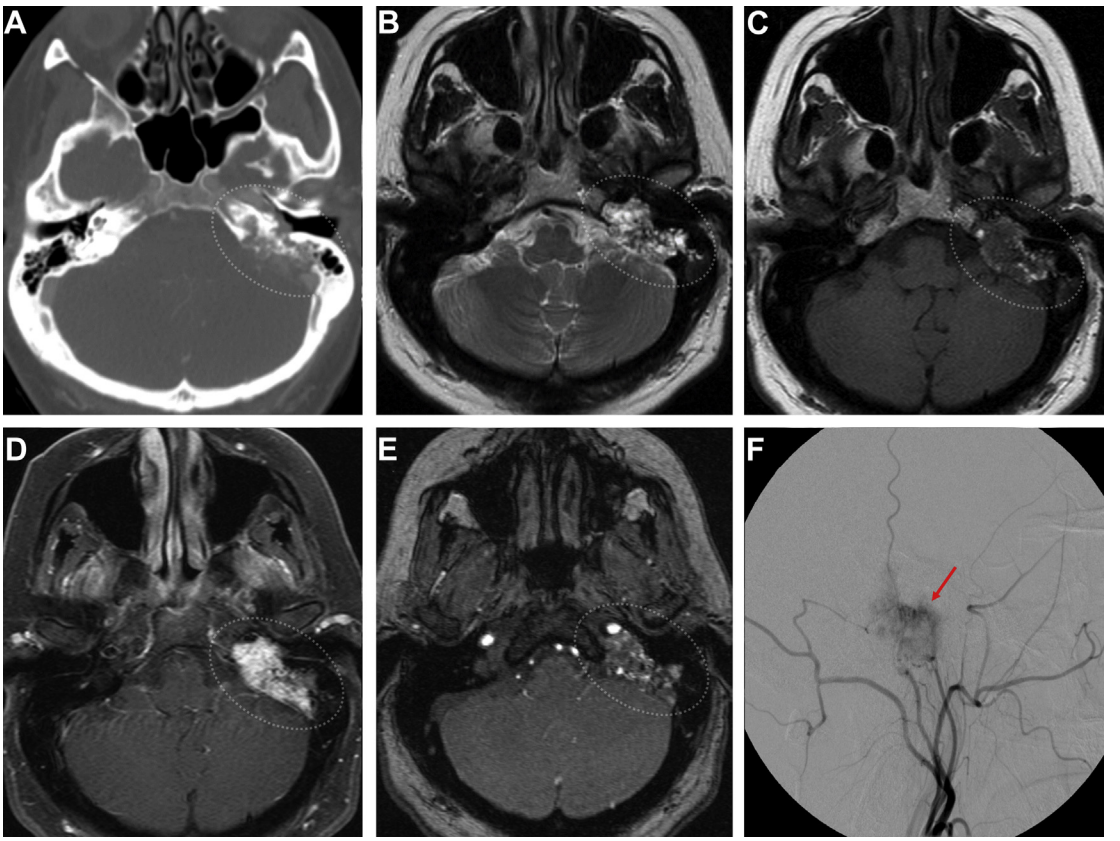

Fig. 19. A 59-year-old woman with endolymphatic sac tumor (*dotted ellipse*) in left temporal bone. (*A*) Axial CT shows moth-eaten type of osteolysis. (*B*) Axial T2WI, (*C*)T1WI, and (*D*) postcontrast T1WI show left temporal bone mass with areas of T1 shortening and intense postcontrast enhancement. (*E*) Axial 3D time-of-flight MRA and (*F*) catheter angiography (left external carotid artery injection) show tumor vascularity (*red arrow*).

Table 2
2012 International Tuberous Sclerosis Complex Consensus Conference diagnostic criteria

1. Genetic diagnostic criteria
   Identification of either TSC1 or TSC2 pathogenic mutation in DNA from normal tissue is sufficient to make a definite diagnosis of TSC. A pathogenic mutation is defined as a mutation that clearly inactivates the function of the TSC1 or TSC2 proteins. Note: 10%–25% of patients with TSC have no mutation identified by conventional genetic testing, and a normal result does not exclude TSC or have any effect on the use of clinical diagnostic criteria to diagnose TSC
2. Clinical diagnostic criteria
   Definitive diagnosis: 2 major features or 1 major plus ≥2 minor features
   Possible diagnosis: 1 major feature or ≥2 minor features

Major feature	Cutaneous • Hypomelanotic macules: ≥3 of at least 5 mm diameter • Angiofibromas (≥3) or fibrous cephalic plaque • Ungual fibromas (≥2) • Shagreen patch Retinal • Multiple retinal hamartomas CNS • Cortical tubers or radial migration lines • Subependymal nodules • SGCA Chest • Cardiac rhabdomyoma • Lymphangioleiomyomatosis Renal • Angiomyolipomas (≥2)
Minor feature	Cutaneous • Confetti skin lesions Orodental • Dental enamel pits (>3) • Intraoral fibromas (≥2) Retinal • Retinal achromic patch Renal • Multiple renal cysts • Nonrenal hamartomas

Ataxia Telangiectasia

Ataxia telangiectasia (AT) is an autosomal recessive condition resulting from a mutation in the *ATM* gene in chromosome 11q22-23. The gene product is involved in DNA repair and apoptosis. Affected individuals present with cerebellar ataxia, immunodeficiency, repeated sinopulmonary infections, increased alpha-fetoprotein level, and telangiectasias in eye and brain. AT is also characterized by radiosensitivity. Lymphoreticular cancers are the most common malignancies in AT. CNS tumors reported in AT are glioma, pilocytic astrocytoma, medulloblastoma, and meningiomas.[19] The imaging features of these tumors are similar to those outside of AT.

Cerebellar volume loss is the hallmark of AT (**Fig. 25**). In particular, superior vermis and lateral cerebellum show the earliest changes.[39] The other reported neuroimaging features are punctate susceptibility low signal foci in the cerebral white matter resulting from microbleeds and capillary telangiectasia, enhancement related to capillary telangiectasias, and white matter FLAIR hyperintense signal changes possibly related to gliosis.[39–42]

Basal Cell Nevus Syndrome (Gorlin Syndrome)

Basal cell nevus syndrome (BCNS) is an AD disorder characterized by mutation in the *PTCH1* tumor suppressor gene in chromosome 9q22.3-31. Multiple basal cell carcinomas (particularly in adolescence) and multiple odontogenic keratocysts (OKCs) are the hallmarks of this syndrome.

Medulloblastoma (MB), especially the desmoplastic subtype, is the most common CNS malignancy reported in BCNS.[43] Imaging findings are similar to the sporadic medulloblastoma tumors. Other reported CNS tumors include oligodendroglioma and craniopharyngioma.[19,43] Meningiomas have also been reported in BCNS, with many of them possibly secondary to cranial radiation. Important neuroimaging clues that point toward Gorlin syndrome are dural calcifications (bilamellar calcifications involving falx and tentorium), OKC in the jaw bones, mandibular coronoid process hyperplasia, scoliosis, frontal bossing, hypertelorism, and cleft lip/palate abnormalities (**Fig. 26**).[19,43,44] The diagnostic criteria recommended by the international colloquium on BCNS is laid out in **Table 3**.[45] The recommendation for neuroimaging surveillance in BCNS is summarized in **Table 4**. Of course, whole-spine imaging should be done in patients with evidence of MB.

Gastrointestinal Polyposis-Related Tumor Syndromes

Cowden syndrome

Cowden syndrome, a phosphatase and tensin homolog (PTEN) hamartoma tumor syndrome, is a group of disorders caused by a mutation in the PTEN gene, located on chromosome 10q23.

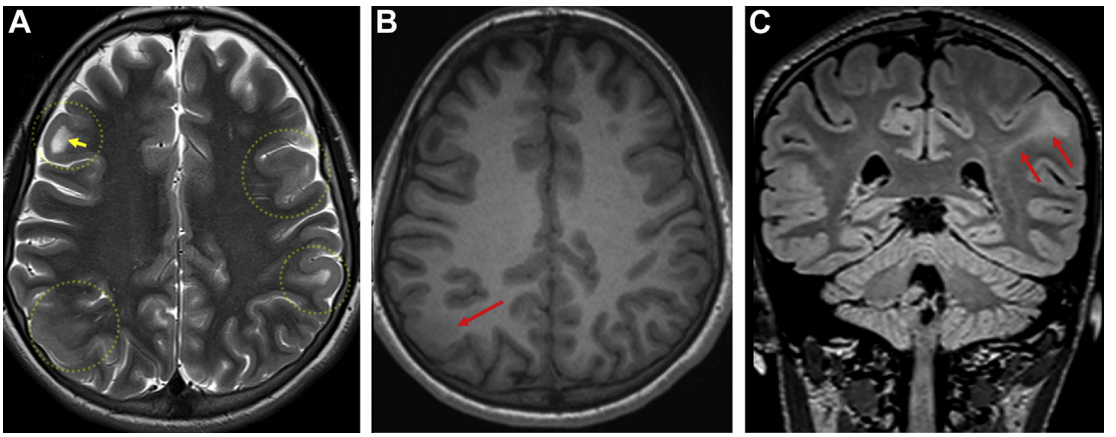

Fig. 20. A 13-year-old girl with TS. (*A*) Axial T2WI and (*B*) T1WI show multiple cortical/subcortical mushroom-shaped tubers (*dotted circles*) with gray-white matter blur in right parietal tuber (*red arrow*). The right frontal subcortical tuber shows cystic change (*yellow arrow*). (*C*) Coronal FLAIR image shows wedge-shaped radial migration line (*red arrows*) extending from tuber to ventricular surface.

These patients have increased risk of breast, endometrial, thyroid, kidney, and colon cancers.[46]

The characteristic CNS lesion in this syndrome is dysplastic cerebellar gangliocytoma (DCG), a hamartomatous tumor, the presence of which in an adult is highly suggestive of Cowden syndrome.[47] DCG appears as a hypodense mass on CT (**Fig. 27**A) with occasional calcification. On MR, DCG has a characteristic striated appearance with thickened folia. The tumor is hypointense on T1WI, hyperintense on T2WI, without postcontrast enhancement, and with facilitated diffusion (**Fig. 27**B–E; **Fig. 28**). On MR spectroscopy, DCG shows decreased NAA and choline levels, with increased lactate level (**Fig. 27**G–I). On FDG-PET/CT, the tumor is hypermetabolic (**Fig. 27**F).[47,48]

Turcot syndrome

Turcot syndrome, also referred to as brain-tumor polyposis syndrome, has 2 subtypes, types 1 and 2. Type 1 is associated with hereditary nonpolyposis colorectal cancer, secondary to germline mutations in mismatch repair genes, and predisposes patients to colorectal, endometrial, gastric, pancreaticobiliary, and genitourinary cancers along with malignant astrocytomas. Type 2 is associated with familial adenomatous polyposis, secondary to mutations in the APC gene, and these patients present with colorectal cancers and skin/osseous lesions along with medulloblastomas.[49–51] On imaging, these tumors look similar to their sporadic counterparts, except that the median age of these patients is less than 20 years.

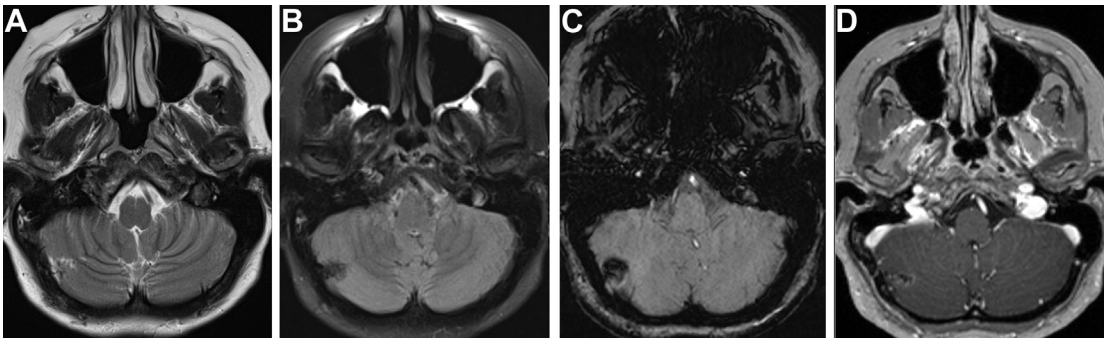

Fig. 21. A 46-year-old woman with TSC2 mutation mosaicism. (*A*) Axial T2WI, (*B*) FLAIR, (*C*) susceptibility-weighted imaging, and (*D*) postcontrast T1WI showing a typical right cerebellar tuber, a wedge-shaped lesion in right cerebellum with susceptibility low signal caused by calcification and heterogeneous postcontrast enhancement.

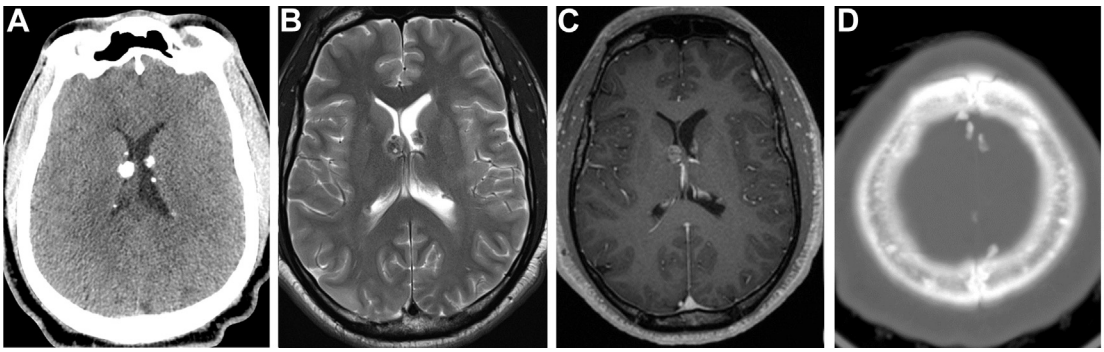

Fig. 22. A 34-year-old patient with TS. (*A*) Axial CT, (*B*) T2WI, and (*C*) postcontrast T1WI show calcified multiple SENs with low T2 signal and postcontrast enhancement. (*D*) Axial CT bone window shows multiple sclerotic foci in the calvarium.

Li-Fraumeni Syndrome

Li-Fraumeni syndrome (LFS) is an AD cancer predisposition disorder, resulting in cancers arising in children and younger adults. This disorder is usually secondary to mutation of tumor suppressor gene TP53, located in the short arm of chromosome17 (17p13.1). Cancers seen in LFS include soft tissue sarcomas, osteosarcomas, premenopausal breast cancers, brain tumors, adrenal cortical carcinomas, leukemias, and lung cancers. Classic LFS diagnosis is based on a combination of clinical presentation and family history, which includes any sarcoma diagnosed before age 45 years, and a first-degree relative with any cancer diagnosed before age 45 years and another first-degree or second-degree relative with any cancer diagnosed before age 45 years or a sarcoma diagnosed at any age. The modified Chompret criteria from 2009 have been developed to identify affected families beyond the classic criteria listed earlier.[52] Lastly, there's an additional set of criteria for Li-Fraumeni–like syndrome.

The CNS tumors seen in LFS include astrocytomas (diffusely infiltrating fibrillary type; WHO grades II–IV) and gliosarcomas, choroid plexus

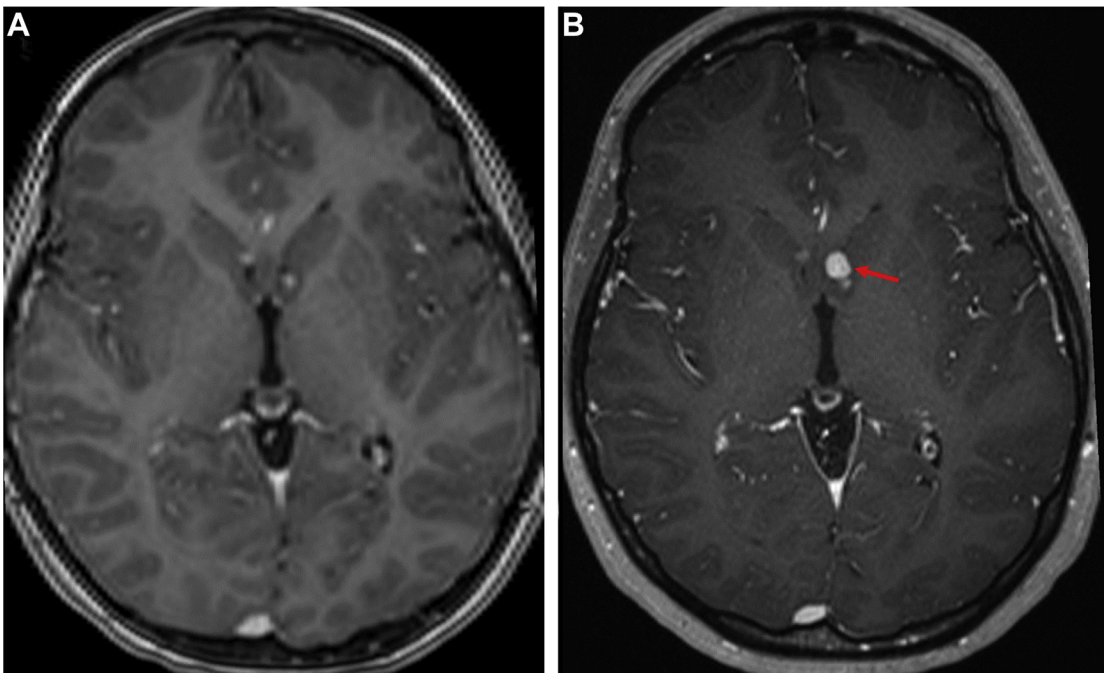

Fig. 23. A 15-year-old girl with TS. (*A*) Axial postcontrast T1WI from 10 years ago shows enhancing SENs. (*B*) One of the SENs (*red arrow*) shows interval enlargement, suggesting transformation into SGCA.

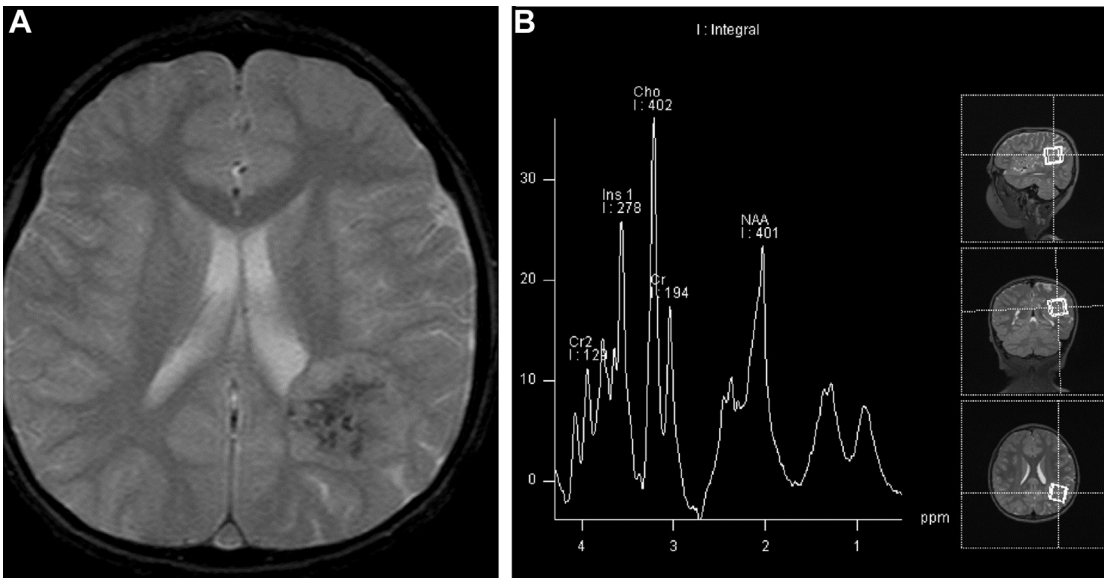

Fig. 24. A 5-year-old patient with non-TS SGCA. (*A*) Axial T2*WI showing a partially calcified left parietal region mass lesion, which was resected and found to be SGCA on histopathology. (*B*) MR spectroscopy revealed increased choline level and decreased N-acetyl aspartate level in the tumor like other neoplasms.

carcinoma, medulloblastoma, and supratentorial primitive neuroectodermal tumors.[53] Imaging findings are similar to sporadic counterparts. Imaging is also an essential part of screening and surveillance of these patents given that almost half of these patients develop an invasive cancer by age 30 years. Both whole-body MR imaging and brain MR imaging scans are recommended annually in addition to clinical and laboratory evaluations.

Multiple Endocrine Neoplasia Type 1

MEN type 1 (MEN1), also referred to commonly by the mnemonic 3Ps syndrome, classically results in

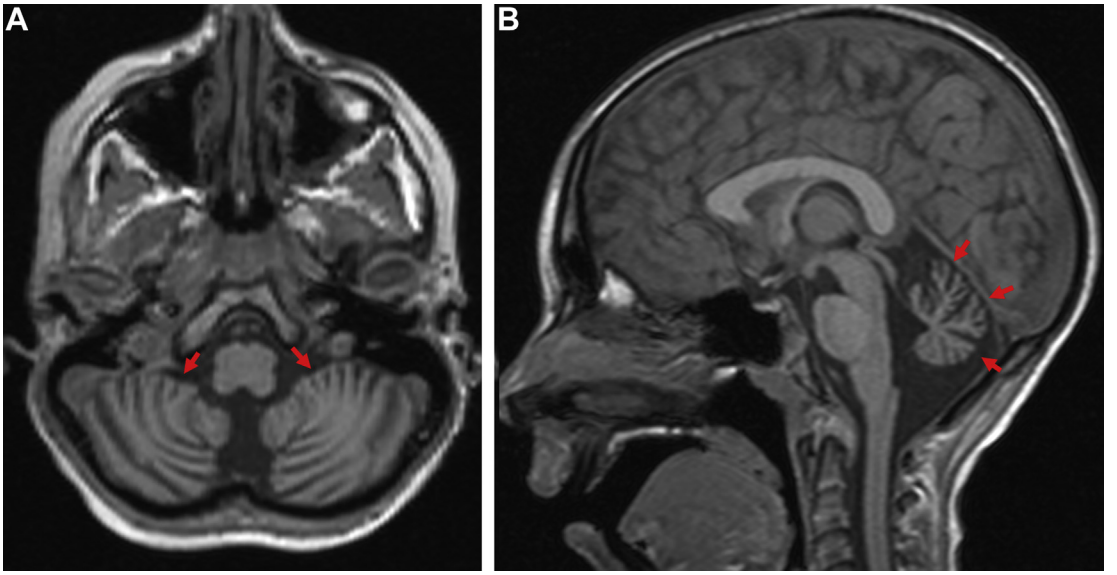

Fig. 25. A 21-year-old patient with AT. (*A*) Axial and (*B*) sagittal T1WI show significant cerebellar parenchymal volume loss, including vermis (*arrows*) with atrophic folia and prominent sulci. The supratentorial parenchyma is spared.

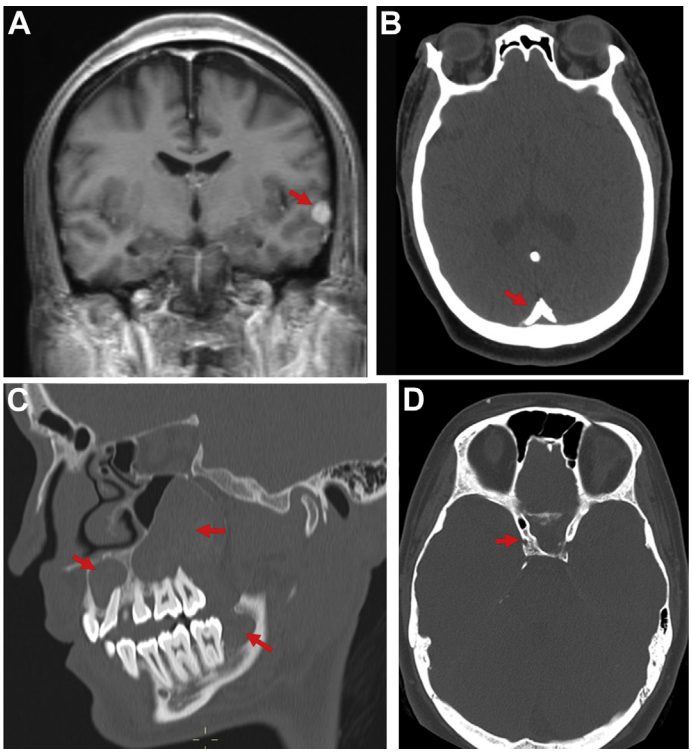

Fig. 26. BCNS. (*A*) Coronal postcontrast T1WI shows a meningioma in left temporal convexity (*arrow*) in a 30-year-old patient with BCNS. (*B*) Axial CT head shows dural calcifications (*arrow*) in the same patient. (*C*) Sagittal oblique reformat of CT face of a 26-year-old patient with BCNS shows multiple OKCs in maxilla and mandible (*arrows*). (*D*) Axial head CT in the same patient shows sellar bridging (*arrow*).

tumors of the parathyroid glands, anterior pituitary, and pancreatic islet cells. It is a high-penetrance AD heritable cancer syndrome, with a prevalence of approximately 2 per 100,000. The basis of oncogenesis in this syndrome is assumed to be the underlying mutation involving the MEN1 gene located on chromosome 11q13, which encodes for the protein menin, thought to be a tumor suppressor gene. Knudson's 2-hit hypothesis is thought to be the underlying mechanism

Table 3
Diagnostic criteria for basal cell nevus syndrome based on the consensus statement from the First International Colloquium (May 2005)

Diagnostic criteria: 2 major criteria (or) 1 major plus 2 minor criteria (or) 1 major criteria plus molecular confirmation	
Major criteria	• Multiple (>2) basal cell carcinomas or 1 before 20 y of age • Odontogenic keratocysts of the jaws before 20 y of age • Palmar or plantar pits • Calcification of the falx cerebri • Medulloblastoma, typically desmoplastic • First-degree relatives with BCNS
Minor criteria	• Rib anomalies (bifid, fused, or markedly splayed ribs) • Cleft lip or palate • Other specific skeletal malformations and radiologic changes (vertebral anomalies, kyphoscoliosis, short fourth metacarpals, postaxial polydactyly) • Macrocephaly • Ovarian/cardiac fibroma • Lymphomesenteric cysts • Ocular abnormalities (ie, strabismus, hypertelorism, congenital cataracts, glaucoma, coloboma)

Table 4
Neuroimaging screening recommendations in Gorlin syndrome

Tumor/Abnormality	Screening Recommendation
Medulloblastoma	Baseline MR imaging brain with contrast followed by annual examination until 8 y
Odontogenic keratocyst	Baseline panorex followed by annual examination until the detection of a jaw cyst. From then, every 6 mo until no jaw cysts for 2 y or until 21 y of age
Scoliosis	Baseline at age 1 y or at time of diagnosis; repeat if symptomatic; if abnormal, repeat every 6 mo

combining the effects of the inherited gene followed by a somatic mutation.[54]

MEN1 diagnosis can be made clinically or on family history, as well as solely from a mutation without any obvious clinical/biochemical manifestations, as summarized in **Table 5**. The most common components of MEN1 are multiple parathyroid tumors causing primary hyperparathyroidism, followed by gastrinomas and pituitary adenomas (**Fig. 29**). However, patients with MEN1 can have multiple tumors other than those in the parathyroid and pituitary, and pancreatic islet cells, the discussion of which is outside the scope of this review.

Neuroradiologists can encounter patients with MEN1 in different settings of both neuro-oncology and neuroendocrine consults secondary to the involvement of parathyroid glands, pituitary, as well as the rare associations with meningiomas and cord ependymomas. MEN1 lesions relevant to neuroradiologists and their prevalence are summarized in **Table 6**.[55]

Pituitary adenomas associated with MEN1 are similar in imaging appearance to sporadic adenomas and can present as both microadenomas ($\leq$10 mm in maximal dimension) and macroadenomas ($\geq$10 mm in maximal dimension). However, adenomas associated with MEN1 are typically larger (more likely to be macroadenomas), more invasive, and difficult to resect surgically.[56] Imaging varies depending on the size of the lesion. The larger macroadenomas are usually isointense to the gray matter on T1/T2 sequences, unless they have calcification, hemorrhage, or cystic changes. On contrast-enhanced sequences, macroadenomas show robust heterogeneous enhancement. In contrast, microadenomas are inconspicuous on nonenhanced sequences and appear slightly hypointense relative to the normal pituitary gland on postcontrast sequences. Also, given that these enhance slowly compared with the pituitary gland, dynamic contrast-enhanced sequences are more sensitive in identifying these lesions.

Primary hyperparathyroidism in MEN1 is usually caused by multiglandular disease. The treatment is usually surgical, which requires the surgeon to do a 4-gland exploration. This requirement limits the role of routine preoperative screening. However, many surgeons prefer to get imaging in patients with atypical clinical presentation/biochemical profiles as well as to evaluate for ectopic glands. US is usually the first-line imaging, with nuclear scintigraphy and multiphase CT being second-line studies. On US, parathyroid adenomas appear as a well-defined, oval, hypoechoic masses adjacent to the thyroid gland, when in eutopic locations. Frequently, an enlarged/prominent vessel referred to as a polar vessel can be seen adjacent to the lesion. However, US is limited in evaluating ectopic locations. (99m)Tc-methoxyisobutylisonitrile (MIBI) planar and single-photon emission CT scintigraphy images of the neck and mediastinum are sensitive for picking up small and ectopic adenomas. In addition, multiphasic CT (also referred to as 4DCT), which involves noncontrast CT and arterial and delayed venous phase acquisitions, is another tool for evaluating these patients, and is preferred by many surgeons because of the excellent anatomic localization, particularly for ectopic adenomas as well as to differentiate from other mimics. In this technique, a parathyroid adenoma is identified by a combination of its shape, location, and enhancement characteristics with early arterial enhancement and washout.

Screening for MEN1-associated tumors is usually done using serum calcium, parathyroid hormone assays, and prolactin measurements annually. Although there is no universal consensus regarding the role of imaging in screening, some experts suggest screening individuals at high risk (such as MEN1 mutant gene carriers) at baseline and every 1 to 3 years using pituitary and abdominal imaging (eg, MR imaging or CT).[55]

Miscellaneous Syndromes

Other CNS-related cancer predisposition syndromes include neurocutaneous melanosis (NCM)[57] (**Fig. 30**), meningioangiomatosis (MA)[58]

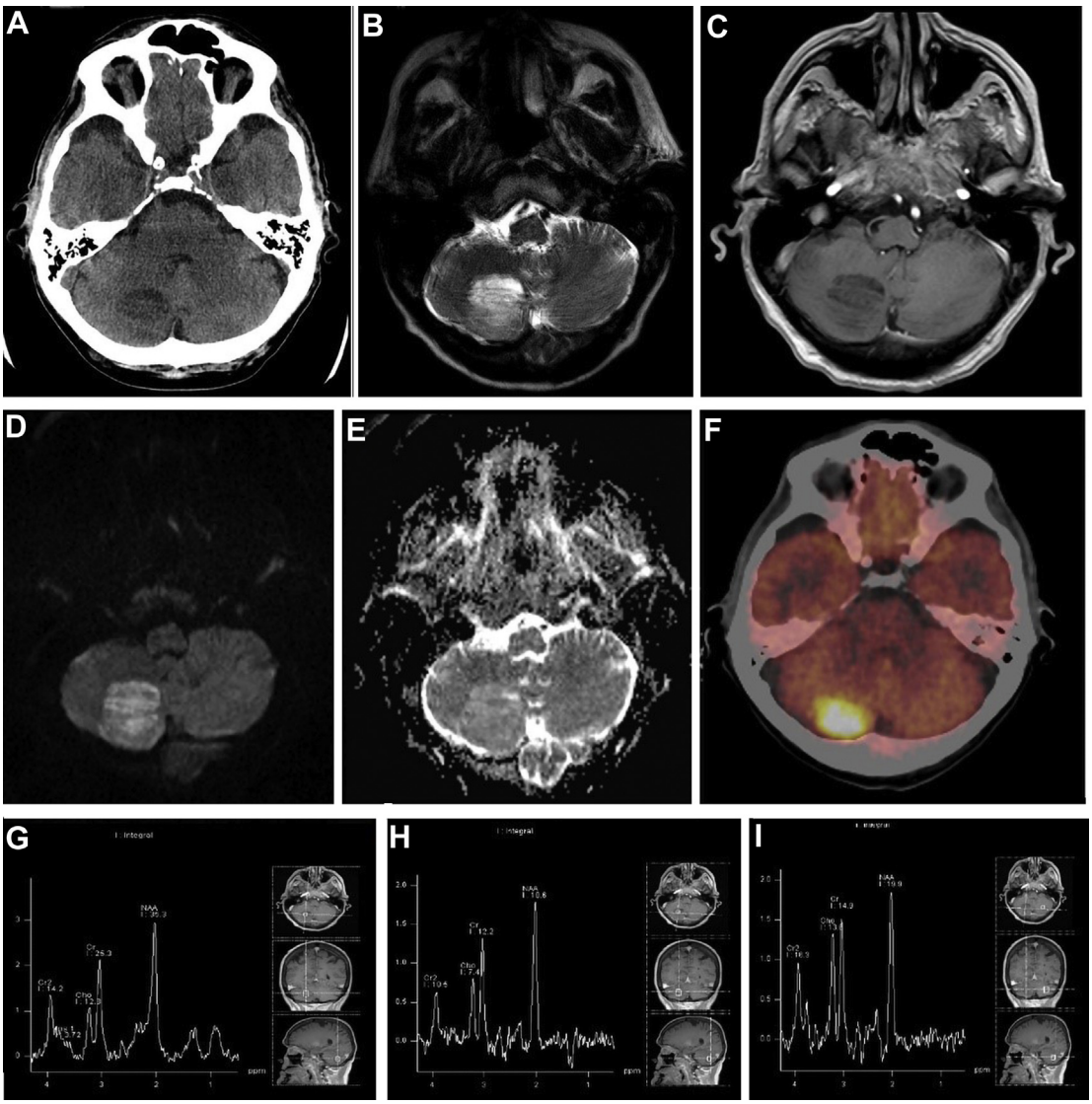

Fig. 27. Dysplastic cerebellar gangliocytoma in a 53-year-old man with Cowden syndrome. (*A*) Axial CT, (*B*) T2WI, (*C*) postcontrast T1WI, (*D*) diffusion-weighted imaging (DWI), and (*E*) ADC images show a CT hypodense, nonenhancing, T2 hyperintense mass in the right cerebellum without restricted diffusion, with striated morphology. (*F*) Fused axial FDG-PET/CT shows hypermetabolic activity of the right cerebellar lesion. MR spectroscopy of the cerebellar mass with (*G*) low and (*H*) intermediate echo time (TE) shows lactate doublet peak inverting in the intermediate TE sequence. (*I*) MR spectroscopy with intermediate TE from contralateral side shown for comparison with normal metabolite peaks.

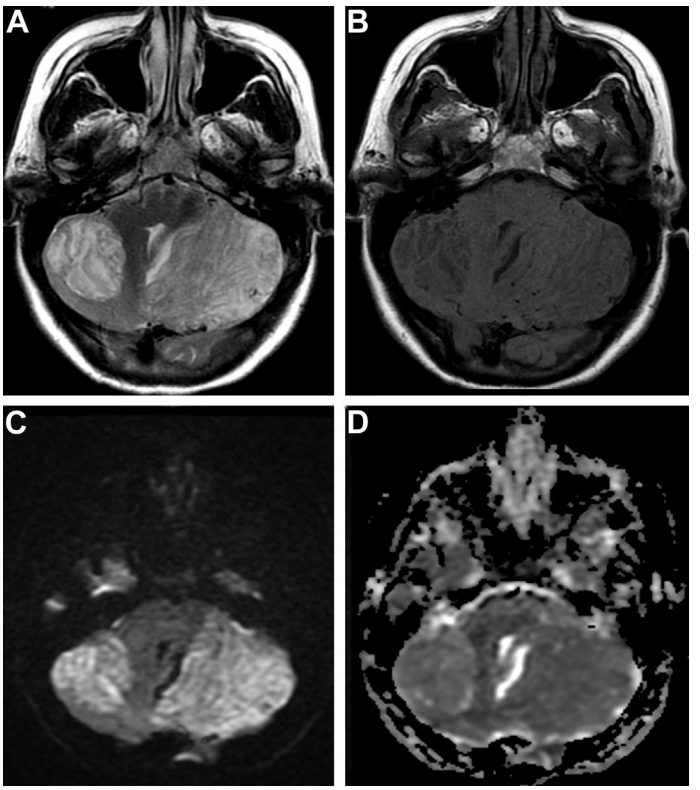

Fig. 28. Bilateral dysplastic cerebellar gangliocytoma in a 40-year-old woman with Cowden syndrome. (*A*) Axial T2WI and (*B*) T1WI shows bilateral T2 hyperintense and T1 hypointense masses with striated appearance on T2WI. (*C*) Axial DWI and (*D*) ADC images show mild restricted diffusion in the cerebellar masses.

Table 5
Diagnostic criteria for multiple endocrine neoplasia type 1

Clinical	A patient with 2 or more MEN1-associated tumors
Familial	A patient with 1 MEN1-associated tumor and a first-degree relative with MEN1
Genetic	An individual with MEN1 mutation who does not have clinical/biochemical manifestations of MEN1

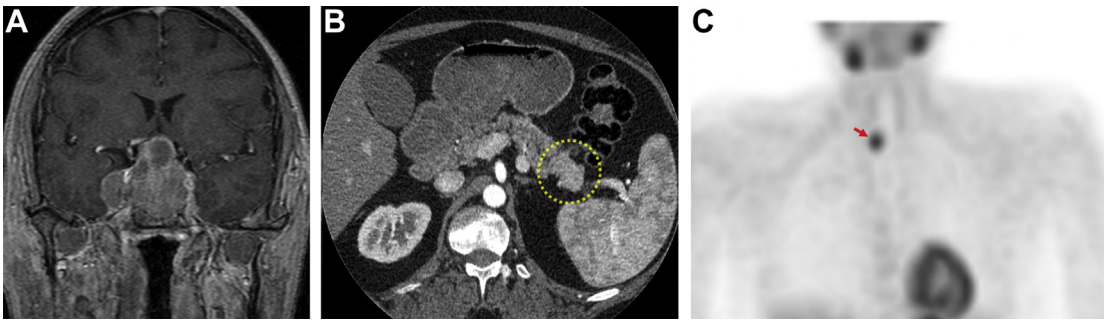

Fig. 29. MEN1. (*A*) Coronal post-T1WI of the brain shows an invasive pituitary macroadenoma with right cavernous sinus invasion in a 40-year-old patient with MEN1. (*B*) Axial CT abdomen in the same patient shows a surgically proven neuroendocrine tumor in the tail of pancreas (*circle*). (*C*) Maximum intensity projection of a delayed (90 minute) ^{99m}Tc-sestamibi scan shows a right inferior parathyroid adenoma (*arrow*) in 49-year-old patient with MEN1.

Table 6
Multiple endocrine neoplasia type 1 lesions relevant to neuroradiologists and their prevalence

Endocrine Lesions	Nonendocrine Lesions
Parathyroid adenomas (90%)	Lipomas (30%)
Anterior pituitary adenomas (30%–40%)	Facial angiofibromas (85%)
Prolactinoma (20%)	Spinal ependymomas (1%)
Prolactinoma plus growth hormone, growth hormone, nonfunctioning (5%)	Meningiomas (8%)
Adrenocorticotropin stimulating (2%)	
Thyroid-stimulating hormone–secreting adenomas (rare)	

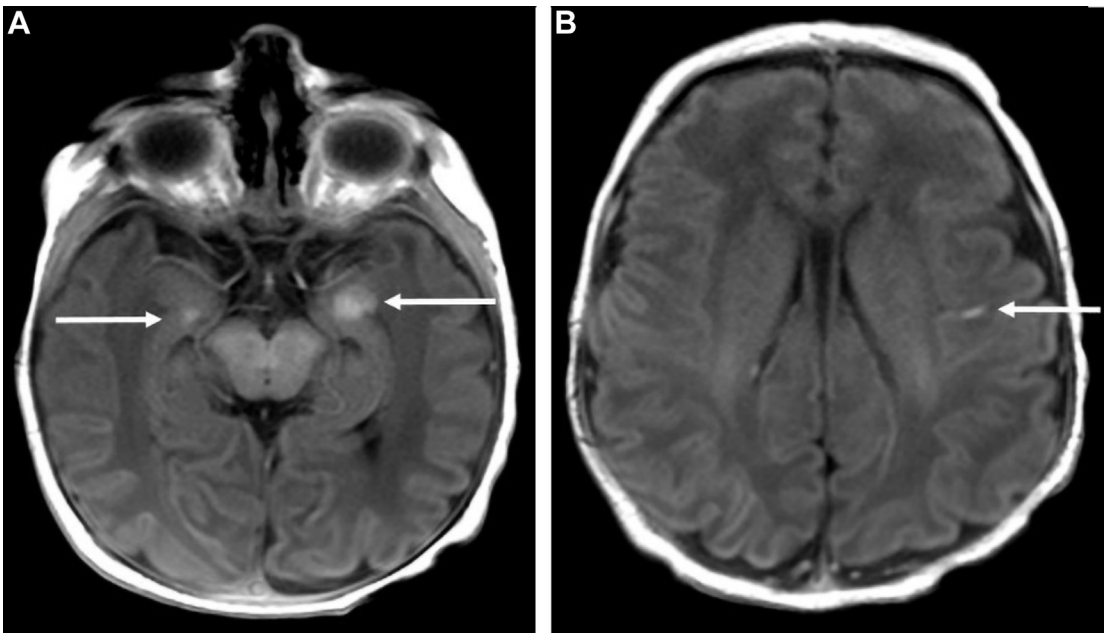

Fig. 30. Parenchymal melanosis in a 2-day-old neonate with neurocutaneous melanosis. Axial T1WI at the level of (*A*) temporal and (*B*) frontal lobes shows T1 hyperintense signal in bilateral amygdala and in left frontal deep white matter corresponding with perivascular melanocytes (*arrows*).

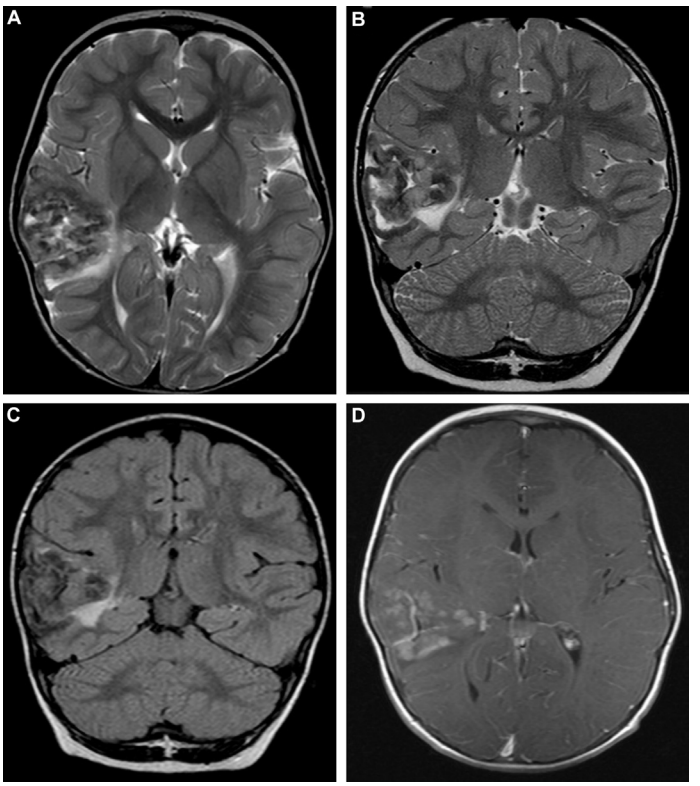

Fig. 31. Meningioangiomatosis in a 3-year-old patient. (*A*) Axial and (*B*) coronal T2WI show thickened dysmorphic right temporal lobe cortex with hypointense T2 signal caused by calcification. (*C*) Coronal FLAIR shows the adjacent white matter edema. (*D*) Axial postcontrast T1WI showing heterogeneous enhancement in the meningioangiomatosis.

Table 7
Miscellaneous central nervous system–related cancer predisposition syndromes

Syndrome	Mutations	Clinical	Tumors	Imaging
NCM	Somatic, NRAS, chromosome 1p13.2	Large (>20 cm) or multiple (>3) congenital nevi Seizure, hydrocephalus with associated clinical features Poor prognosis for both leptomeningeal melanocytosis and leptomeningeal melanomatosis	CNS: parenchymal and leptomeningeal melanoma Leptomeningeal melanomatosis Skin: malignant melanoma	Ideally MR imaging done before 6 mo of age in suspected infants, with follow-up surveillance scans Can be normal Meningeal Leptomeningeal focal melanocytic neoplasms: T1 shortening Leptomeningeal melanocytosis: T1 shortening with or without diffuse enhancement Leptomeningeal melanomatosis: T1 shortening with diffuse enhancement FLAIR sequence may show diffuse sulcal hyperintensity in leptomeningeal melanocytosis and melanomatosis Parenchymal Parenchymal melanosis: T1 shortening without enhancement, amygdala and cerebellum are most common sites

(*continued on next page*)

Table 7
(*continued*)

Syndrome	Mutations	Clinical	Tumors	Imaging
				Malignant melanoma: T1 shortening, enhancement can be heterogeneous
MA	Some are associated with NF2	Seizure	Benign hamartomatous malformation	Cortical/subcortical lesion, often shows calcification. Variable enhancement of the leptomeninges and the cortical component. There can be edema in the subjacent white matter
RTPS	*RTPS1 SMARCB1* *RTPS2*: *SMARCA4*	Typically present at very young age	Brain: atypical teratoid/rhabdoid tumor Rhabdoid tumor of the kidney and other organs Schwannoma	Heterogeneous in T1WI and T2WI, may show hemorrhage and cysts. Restricted diffusion, heterogeneous enhancement
MAS	Germline, *CDKN2A* tumor suppressor gene, chromosome 9p21	Seizure, cutaneous lesions from melanoma	Melanoma, astrocytoma, occasionally meningiomas, schwannoma, and neurofibroma	Imaging features are similar to the tumors seen in nonsyndromic patients
CC	*PRKAR1A*, chromosome 17q22–24 Chromosome 2p16	Pigmented lesions of the skin and mucosa, cardiac myxoma: stroke, cardiac failure, sudden death, acromegaly,	Cardiac myxoma, cutaneous and other soft tissue myxomas. Endocrine tumors: pituitary, adrenocortical, thyroid. Testicular,	Imaging features of pituitary adenomas are similar to the tumors seen in nonsyndromic patients

		Cushing, precocious puberty	ovarian and breast tumors. Pancreatic tumors, and so forth	
RTS	*CREBBP, EP300*	Mental retardation, behavioral problems, growth retardation, and multiple congenital anomalies, especially of the face and distal limbs, keloids	Meningioma, pilomatrixoma	Imaging features are similar to the tumors seen in nonsyndromic patients

Abbreviations: CC, Carney complex; *CDKN2A*, cyclin-dependent kinase inhibitor 2A; *CREBBP*, CREB-binding protein; *EP*, E1A-binding protein p300; MA, meningioangiomatosis; *NRAS*, N-Ras proto-oncogene; *PRKAR1A*, protein kinase cAMP-dependent type I regulatory subunit alpha; *SMARCA4/B1*, SWI/SNF-related, matrix-associated, actin-dependent regulator of chromatin.

(**Fig. 31**), rhabdoid tumor predisposition syndromes (RTPS),[59] melanoma-astrocytoma syndrome (MAS),[60] Carney complex,[61] and Rubinstein-Taybi syndrome (RTS).[62] The significant characteristics of these syndromes are summarized in **Table 7**.

CLINICS CARE POINTS

- Heritable and non-heritable cancer syndromes affecting the central nervous system have distinctive underlying mutations and molecular pathways, resulting in a myriad of both tumors, and non-tumorous lesions, with unique histopathological and imaging features.
- Recent advances in radiogenomics and understanding of cancer pathways, have led to renewed emphasis on screening and early diagnosis, targeting for innovating therapies, optimizing surveillance for monitoring therapies and follow up with imaging playing a central role in many of the above.
- Both organ specific and whole body protocols using multimodality imaging represent a crucial tool in optimizing imaging for both lesions involving the brain and spinal cord, as well as lesions outside the central nervous system, which requires leveraging the advancements in scanners and optimizing protocols.
- In addition to their expertise in imaging findings, radiologists need to have familiarity with radiogenomics and molecular cancer pathways to better serve both patients and clinicians.

DISCLOSURE

None.

REFERENCES

1. Greer MLC, Voss SD, States LJ. Pediatric cancer predisposition imaging: focus on whole-body MRI. Clin Cancer Res 2017;23(11):e6–13.
2. Kresak J, Walsh M. Neurofibromatosis: a review of NF1, NF2, and schwannomatosis. J Pediatr Genet 2016;05(02):098–104.
3. Lin J, Martel W. Cross-sectional imaging of peripheral nerve sheath tumors. Am J Roentgenol 2001; 176(1):75–82.
4. Pascual-Castroviejo I, Pascual-Pascual SI, Velazquez-Fragua R, et al. Familial spinal neurofibromatosis. Neuropediatrics 2007;38(2):105–8.
5. Woodruff J. Pathology of tumors of the peripheral nerve sheath. Am J Med Genet 1999;89(1):23–30.
6. Jee W-H, Oh S-N, McCauley T, et al. Extraaxial neurofibromas versus neurilemmomas: discrimination with MRI. Am J Roentgenol 2004;183(3):629–33.
7. Kornreich L, Blaser S, Schwarz M, et al. Optic Pathway glioma: correlation of imaging findings with the presence of neurofibromatosis. AJNR Am J Neuroradiol 2001;22(10):1963–9.
8. Binning MJ, Liu JK, Kestle JRW, et al. Optic pathway gliomas: A review. Neurosurg Focus 2007;23(5):1–8.
9. DiPaolo DP, Zimmerman RA, Rorke LB, et al. Neurofibromatosis type 1: Pathologic substrate of high-signal-intensity foci in the brain. Radiology 1995; 195(3):721–4.
10. Itoh T, Magnaldi S, White RM, et al. Neurofibromatosis type 1: The evolution of deep gray and white matter MR abnormalities. AJNR Am J Neuroradiol 1994;15(8):1513–9.
11. Cairns AG, North KN. Cerebrovascular dysplasia in neurofibromatosis type 1. J Neurol Neurosurg Psychiatry 2008;79(10):1165–70.
12. Baser ME, Friedman JM, Joe H, et al. Empirical development of improved diagnostic criteria for neurofibromatosis 2. Genet Med 2011;13(6):576–81.
13. Evans DGR. Neurofibromatosis type 2 (NF2): A clinical and molecular review. Orphanet J Rare Dis 2009;4(1):1–11.
14. Evans DG, King AT, Bowers NL, et al. Identifying the deficiencies of current diagnostic criteria for neurofibromatosis 2 using databases of 2777 individuals with molecular testing. Genet Med 2019;21(7):1525–33.
15. Asthagiri AR, Parry DM, Butman JA, et al. Neurofibromatosis type 2. Lancet 2009;373(9679):1974–86.
16. Coy S, Rashid R, Stemmer-Rachamimov A, et al. An update on the CNS manifestations of neurofibromatosis type 2. Acta Neuropathol 2020;139(4):643–65.
17. Evans DG, Bowers NL, Tobi S, et al. Schwannomatosis: A genetic and epidemiological study. J Neurol Neurosurg Psychiatry 2018;1215–9. https://doi.org/10.1136/jnnp-2018-318538.
18. Binderup MLM, Bisgaard ML, Harbud V, et al. Von Hippel-Lindau disease (vHL). National clinical guideline for diagnosis and surveillance in Denmark. 3rd edition. Dan Med J 2013;60(12):B4763.
19. Vijapura C, Saad Aldin E, Capizzano AA, et al. Genetic syndromes associated with central nervous system tumors. Radiographics 2017;37(1): 258–80.
20. Lonser RR, Glenn GM, Walther M, et al. von Hippel-Lindau disease. Lancet 2003;361(9374):2059–67.
21. Wanebo JE, Lonser RR, Glenn GM, et al. The natural history of hemangioblastomas of the central nervous

system in patients with von Hippel-Lindau disease. J Neurosurg 2003;98(1):82–94.
22. Lee SR, Sanches J, Mark AS, et al. Posterior fossa hemangioblastomas: MR imaging. Radiology 1989; 171(2):463–8.
23. Leung RS, Biswas SV, Duncan M, et al. Imaging features of von Hippel-Lindau disease. Radiographics 2010;28(1):65–79 [quiz: 323].
24. Binderup MLM, Stendell A-S, Galanakis M, et al. Retinal hemangioblastoma: prevalence, incidence and frequency of underlying von Hippel-Lindau disease. Br J Ophthalmol 2018;102(7):942–7.
25. Wiley HE, Krivosic V, Gaudric A, et al. MANAGEMENT OF RETINAL HEMANGIOBLASTOMA IN VON HIPPEL-LINDAU DISEASE. Retina 2019; 39(12):2254–63.
26. Lonser RR, Kim HJ, Butman JA, et al. Tumors of the endolymphatic sac in von Hippel-Lindau disease. N Engl J Med 2004;350(24):2481–6.
27. Shanbhogue KP, Hoch M, Fatterpaker G, et al. von Hippel-Lindau disease: review of genetics and imaging. Radiol Clin North Am 2016;54(3):409–22.
28. Melean G, Sestini R, Ammannati F, et al. Genetic insights into familial tumors of the nervous system. Am J Med Genet C Semin Med Genet 2004;129C(1): 74–84.
29. Northrup H, Krueger DA. International Tuberous Sclerosis Complex Consensus Group. Tuberous sclerosis complex diagnostic criteria update: recommendations of the 2012 International Tuberous Sclerosis Complex Consensus Conference. Pediatr Neurol 2013;49(4):243–54.
30. Braffman BH, Bilaniuk LT, Naidich TP, et al. MR imaging of tuberous sclerosis: pathogenesis of this phakomatosis, use of gadopentetate dimeglumine, and literature review. Radiology 1992;183(1):227–38.
31. Manara R, Bugin S, Pelizza MF, et al. Genetic and imaging features of cerebellar abnormalities in tuberous sclerosis complex: more insights into their pathogenesis. Dev Med Child Neurol 2018;60(7): 724–5.
32. Manoukian SB, Kowal DJ. Comprehensive imaging manifestations of tuberous sclerosis. AJR Am J Roentgenol 2015;204(5):933–43.
33. Altman NR, Purser RK, Post MJD. Tuberous sclerosis: characteristics at CT and MR imaging. Radiology 1988;167(2):527–32.
34. DiMario FJ. Brain abnormalities in tuberous sclerosis complex. J Child Neurol 2004;19(9):650–7.
35. Inoue Y, Nemoto Y, Murata R, et al. CT and MR imaging of cerebral tuberous sclerosis. Brain Dev 1998; 20(4):209–21.
36. Waga S, Yamamoto Y, Kojima T, et al. Massive hemorrhage in tumor of tuberous sclerosis. Surg Neurol 1977;8(2):99–101.
37. Sener RN. Tuberous sclerosis: diffusion MRI findings in the brain. Eur Radiol 2002;12(1):138–43.
38. de Carvalho Neto A, Gasparetto EL, Bruck I. Subependymal giant cell astrocytoma with high choline/creatine ratio on proton MR spectroscopy. Arq Neuropsiquiatr 2006;64(3B):877–80.
39. Tavani F, Zimmerman RA, Berry GT, et al. Ataxia-telangiectasia: The pattern of cerebellar atrophy on MRI. Neuroradiology 2003;45(5):315–9.
40. Sardanelli F, Parodi RC, Ottonello C, et al. Cranial MRI in ataxia-telangiectasia. Neuroradiology 1995; 37(1):77–82.
41. Sahama I, Sinclair K, Pannek K, et al. Radiological imaging in ataxia telangiectasia: A review. Cerebellum 2014;13(4):521–30.
42. Lin DDM, Barker PB, Lederman HM, et al. Cerebral abnormalities in adults with ataxia-telangiectasia. AJNR Am J Neuroradiol 2014;35(1):119–23.
43. Thalakoti S, Geller T. 1st edition. Basal cell nevus syndrome or Gorlin syndrome, vol. 132. The Netherlands: Elsevier B.V.; 2015.
44. Leonardi R, Caltabiano M, Lo Muzio L, et al. Bilateral hyperplasia of the mandibular coronoid processes in patients with nevoid basal cell carcinoma syndrome: An undescribed sign [4]. Am J Med Genet 2002;110(4):400–3.
45. Bree AF, Shah MR. Consensus statement from the first international colloquium on basal cell nevus syndrome (BCNS). Am J Med Genet A 2011;155(9): 2091–7.
46. Pilarski R, Burt R, Kohlman W, et al. Cowden syndrome and the PTEN hamartoma tumor syndrome: Systematic review and revised diagnostic criteria. J Natl Cancer Inst 2013;105(21):1607–16.
47. Klisch J, Juengling F, Spreer J, et al. Lhermitte-Duclos disease: Assessment with MR imaging, positron emission tomography, single-photon emission CT, and MR spectroscopy. AJNR Am J Neuroradiol 2001;22(5):824–30.
48. Awwad EE, Levy E, Martin DS, et al. Atypical MR appearance of Lhermitte-Duclos disease with contrast enhancement. AJNR Am J Neuroradiol 1995;16(8):1719–20.
49. Bronner MP. Gastrointestinal inherited polyposis syndromes. Mod Pathol 2003;16(4):359–65.
50. Lebrun C, Olschwang S, Jeannin S, et al. Turcot syndrome confirmed with molecular analysis. Eur J Neurol 2007;14(4):470–2.
51. Mullins KJ, Rubio A, Myers SP, et al. Malignant ependymomas in a patient with Turcot's Syndrome: Case report and management guidelines. Surg Neurol 1998;49(3):290–4.
52. Malkin D. Li-fraumeni syndrome. Genes and Cancer 2011;2(4):475–84.
53. Orr BA, Clay MR, Pinto EM, et al. An update on the central nervous system manifestations of Li–Fraumeni syndrome. Acta Neuropathol 2020; 139(4):669–87.

54. Lemos MC, Thakker RV. Multiple endocrine neoplasia type 1 (MEN1): analysis of 1336 mutations reported in the first decade following identification of the gene. Hum Mutat 2008;29(1):22–32.
55. Thakker RV, Newey PJ, Walls GV, et al. Clinical practice guidelines for multiple endocrine neoplasia type 1 (MEN1). J Clin Endocrinol Metab 2012;97(9):2990–3011.
56. Burgess JR, Shepherd JJ, Parameswaran V, et al. Spectrum of pituitary disease in multiple endocrine neoplasia type 1 (MEN 1): clinical, biochemical, and radiological features of pituitary disease in a large MEN 1 kindred. J Clin Endocrinol Metab 1996;81(7):2642–6.
57. Ramaswamy V, Delaney H, Haque S, et al. Spectrum of central nervous system abnormalities in neurocutaneous melanocytosis. Dev Med Child Neurol 2012;54(6):563–8.
58. Aizpuru RN, Quencer RM, Norenberg M, et al. Meningioangiomatosis: clinical, radiologic, and histopathologic correlation. Radiology 1991;179(3):819–21.
59. Sredni ST, Tomita T. Rhabdoid tumor predisposition syndrome. Pediatr Dev Pathol 2015;18(1):49–58.
60. Chan AK, Han SJ, Choy W, et al. Familial melanoma-astrocytoma syndrome: Synchronous diffuse astrocytoma and pleomorphic xanthoastrocytoma in a patient with germline CDKN2A/B deletion and a significant family history. Clin Neuropathol 2017;36(5):213–21.
61. Correa R, Salpea P, Stratakis CA. Carney complex: an update. Eur J Endocrinol 2015;173(4):M85–97.
62. Boot MV, van Belzen MJ, Overbeek LI, et al. Benign and malignant tumors in Rubinstein–Taybi syndrome. Am J Med Genet A 2018;176(3):597–608.